

Explaining the Equatorial Pacific Thermocline Response to Climate Change with a Model  
Hierarchy

Matthew T. Luongo<sup>1,2\*</sup>, Shang-Ping Xie<sup>3</sup>, Ian Eisenman<sup>3</sup>, Shantong Sun<sup>4</sup>, & Kyle Armour<sup>2,5</sup>

1. Cooperative Institute for Climate, Ocean, & Ecosystem Studies, University of Washington, Seattle, WA, USA
2. School of Oceanography, University of Washington, Seattle, WA, USA
3. Scripps Institution of Oceanography, UC San Diego, La Jolla, CA, USA
4. Laoshan Laboratory, Qingdao, China
5. Department of Atmospheric & Climate Science, University of Washington, Seattle, WA, USA

\* mluongo@uw.edu

This manuscript is a pre-print submitted to EarthArXiv.

The pre-print has been submitted for review to *Journal of Geophysical Research: Oceans*.

Subsequent versions may have altered content.

# Explaining the Equatorial Pacific Thermocline Response to Climate Change with a Model Hierarchy

Matthew T. Luongo<sup>1,2</sup>, Shang-Ping Xie<sup>3</sup>, Ian Eisenman<sup>3</sup>, Shantong Sun<sup>4</sup>, &  
Kyle C. Armour<sup>2,5</sup>

<sup>1</sup>Cooperative Institute for Climate, Ocean, & Ecosystem Studies, University of Washington, Seattle, WA

<sup>2</sup>School of Oceanography, University of Washington, Seattle, WA

<sup>3</sup>Scripps Institution of Oceanography, UC San Diego, La Jolla, CA

<sup>4</sup>Laoshan Laboratory, Qingdao, China

<sup>5</sup>Department of Atmospheric & Climate Science, University of Washington, Seattle, WA

## Key Points:

- Climate models can largely recreate observed equatorial Pacific subsurface temperature trends from 1958-2020
- The observed subsurface temperature change is due to wind changes, remote SST changes, and local SST changes
- Our results suggest that canonical drivers of the equatorial Pacific response to climate change have been misattributed

---

Corresponding author: M.T. Luongo, [mluongo@uw.edu](mailto:mluongo@uw.edu)

**Abstract**

Most studies of the equatorial Pacific response to anthropogenic forcing have focused on patterns of sea surface temperature (SST) change. However, similar SST patterns can be consistent with a range of different subsurface responses, each with differing physical and biogeochemical implications. While historical observation and climate model mismatches have been suggested in the literature, we show that model simulations can largely capture the observed 1958-2020 subsurface temperature trend in the equatorial thermocline. We then analyze a hierarchy of idealized model simulations, consisting of fully-coupled, mechanically-decoupled, ocean-only, and reduced gravity models, to understand which ocean dynamics contribute to this response. We show that the response of the thermocline to idealized climate change can be explained by a combination of decadal Bjerknes-like momentum dynamics and radiatively-forced buoyancy-driven dynamics. We further decompose the buoyancy-driven pattern into a pattern driven by remote, subtropical SST forcing and a pattern driven by local, equatorial SST forcing. The remote-SST-forced pattern of thermocline warming shows the signature of dynamic and thermodynamic subtropical cell adjustments. Meanwhile, increased stratification in the local-SST-forced pattern both coherently shoals the thermocline and relaxes thermocline tilt to largely cool the thermocline. Considered together, we recreate the long-term subsurface equatorial Pacific response to idealized greenhouse gas forcing as a linear combination of (i) wind-stress-driven changes, (ii) remote buoyancy-driven changes, and (iii) local buoyancy-driven changes. To conclude we discuss implications for recent temperature trends, revisit canonical theories of the ocean dynamical thermostat, and show the insensitivity of forced responses to forcing geography.

**Plain Language Summary**

While most research on the equatorial Pacific response to climate change has focused on surface ocean temperatures, different ocean circulation changes can lead to similar surface temperature patterns. In this work we show that climate model simulations can largely capture the observed equatorial Pacific subsurface temperature response to climate change on centennial timescales. We then use a series of idealized modeling simulations, from a complex global climate model to a simple primitive equation model, to explain the ocean dynamics that create this response. Our central result is that the equatorial Pacific subsurface temperature response to climate change is a simple linear sum

of the ocean’s response to changes in winds, changes in remote sea surface temperature patterns, and changes in local sea surface temperature patterns. We explore the dynamics of each of these individual responses. Last, we show that this understanding does not explain subsurface temperature patterns since the late 1970s, and we discuss how our results suggest a reinterpretation of commonly held assumptions of how the equatorial ocean will respond to climate change.

## 1 Introduction

A strong zonal gradient in sea surface temperature (SST) exists in the equatorial Pacific between the western Pacific warm pool and the eastern Pacific cold tongue. This zonal SST gradient is the most obvious manifestation of a series of coupled atmospheric and oceanic processes that connect easterly trade winds, westward surface currents, an eastward subsurface return flow within an upward tilting thermocline, and upwelling of cool sub-thermocline waters in the eastern equatorial Pacific (Bjerknes, 1969; Wyrtki, 1975). Variability in the equatorial Pacific mean state shifts the location of atmospheric deep convection and excites planetary waves that propagate to the extratropics to affect global climate (Horel & Wallace, 1981). Across a broad range of time-scales, from interannual changes of the El Niño-Southern Oscillation (ENSO, Philander, 1983) to decadal changes of the Pacific Decadal Oscillation (PDO, Mantua et al., 1997), the equatorial Pacific is a key driver and pacemaker for global climate (e.g., Kosaka & Xie, 2016).

Given its outsize influence on Earth’s climate, it is critical to understand how the equatorial Pacific will respond to anthropogenic greenhouse gas emissions (e.g., DiNezio et al., 2009; Xie et al., 2010). A key question, which has received much attention and debate, is: How will the equatorial zonal SST gradient change in the future? Constraints from atmospheric thermodynamics have been primarily invoked in support of a decreasing gradient (i.e., more warming in the eastern than western equatorial Pacific): enhanced evaporative cooling in the warmer western Pacific can more readily balance anomalous radiative forcing than the cooler eastern Pacific (Knutson & Manabe, 1995; Merlis & Schneider, 2011), and the atmospheric Walker circulation slow-down implied by specific humidity changes would relax thermocline tilt (Vecchi & Soden, 2007). Meanwhile, Clement et al. (1996) and Seager and Murtugudde (1997) proposed the “ocean dynamical thermostat” and suggested that the zonal SST gradient should in fact increase. The thermostat theory suggests that the eastern equatorial Pacific should warm by less than the

81 rest of the tropics because upwelled equatorial waters, originating in the extratropics and  
82 reaching the equator via the oceanic subtropical cells (STCs: Liu, 1994; McCreary Jr &  
83 Lu, 1994), will not show an effect of surface forcing until some time later. More recently,  
84 several studies have suggested that this debate is simply a matter of time-scales, with  
85 a brief strengthening of the zonal gradient eventually giving way to a long-term weak-  
86 ening (Luo et al., 2017; Heede et al., 2020, 2021; Heede & Fedorov, 2021).

87 However, the continued inability of coupled models to recreate recent historical equa-  
88 torial Pacific SST trends (Coats & Karnauskas, 2017; Seager et al., 2019, 2022; Watan-  
89 abe et al., 2021; Wills et al., 2022) calls into question this seeming resolution. While ob-  
90 servational products suggest that the western Pacific has warmed and central-eastern Equa-  
91 torial Pacific has cooled since the beginning of the satellite era (e.g., Karnauskas et al.,  
92 2009; Solomon & Newman, 2012; Seager et al., 2019; Wills et al., 2022), over that same  
93 period the vast majority of coupled global climate models (GCMs) show enhanced warm-  
94 ing in the eastern Pacific relative to the western Pacific. Many studies have attempted  
95 to explain the mismatch between observed and modeled equatorial Pacific SST trends,  
96 pointing to i) mismatched internal variability (e.g., Laepple & Huybers, 2014; Olonscheck  
97 et al., 2020; Watanabe et al., 2021; Heede & Fedorov, 2023; Jiang et al., 2024a), ii) in-  
98 correct model processes that could otherwise create observed trends (e.g., McGregor et  
99 al., 2018; Baldwin et al., 2021; Dong et al., 2022; Kang et al., 2023; Hwang et al., 2024),  
100 and iii) systematic biases in model mean states that do not allow a forced response to  
101 establish (Seager et al., 2019, 2022; Heede & Fedorov, 2023; Jiang et al., 2024a, 2025).

102 While the mismatch between observed and modeled historical equatorial SST has  
103 been extensively discussed, the subsurface equatorial temperature response to climate  
104 change has been relatively understudied. This top-down focus on SST alone potentially  
105 obfuscates important subsurface oceanic adjustments (e.g., Clement et al., 1996; Vec-  
106 chi & Soden, 2007) that have helped to shape the SST response. For instance, despite  
107 comprising entirely different subsurface dynamics, both decreased thermocline tilt (Vecchi  
108 & Soden, 2007; Luongo et al., 2023) and coherent thermocline deepening (Luongo et al.,  
109 2025) could theoretically lead to an El Niño-like SST pattern.

110 Following Jiang et al. (2025), we show a composite of the 1958-2020 subsurface equa-  
111 torial (meridionally averaged from 5°S-5°N) Pacific temperature trend from two obser-  
112 vational products [EN04 (1958-2020, Good et al., 2013) & Ishii (1958-2012, Ishii & Ki-

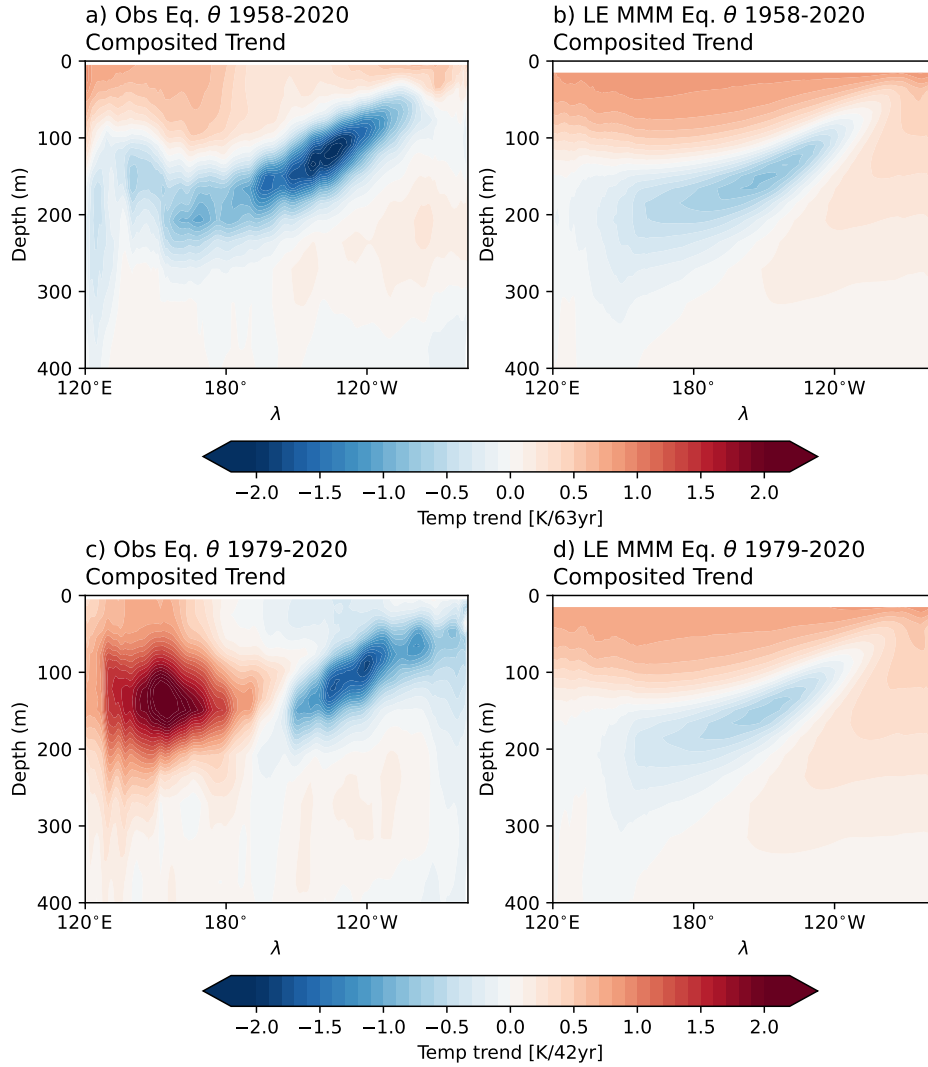


**Figure 1.** a) 1958-2020 equatorial temperature ( $\theta$ ) trend composited from EN04, Ishii, ORAS5, and SODA2.2.4 observational products. b) Multi-model mean equatorial  $\theta$  from 11 large ensemble simulations over 1958-2020. c) As in panel a) but for the period of 1979-2020. d) As in panel b) but for the period of 1979-2020.

113 moto, 2009)] and two ocean reanalyses [ORAS5 (1958-2020, Zuo et al., 2019) & SODA2.2.4  
114 (1958-2010, Carton & Giese, 2008)] (Figure 1a). The most obvious feature of subsurface  
115 equatorial temperatures over the past 60 years is a broad thermocline cooling. Due to  
116 the upward and eastward tilt of the thermocline, this cooling is around 250m deep in the  
117 west-central Pacific and around 50m deep in the eastern Pacific. Maximum cooling oc-  
118 curs between 150°W-120°W from approximately 100-175m. While the cooling is the most  
119 eye-catching feature in this observational pattern, we also note a broad surface warm-  
120 ing, which is minimized in the central Pacific and extends deeper in the western Pacific  
121 than eastern Pacific, and a sub-thermocline warming in the eastern Pacific. These fea-  
122 tures are largely shared by individual observational products (Figure S1).

123 The observed 1958-2020 subsurface temperature trend in Figure 1a is similar to the  
124 1951-2010 trend pattern in Watanabe et al. (2021). We note, however, that the specific  
125 time period considered greatly influences this pattern: Figure 1a is markedly different  
126 than both the 1979-2020 pattern (Figure 1c) and the 1979-2013 pattern (Watanabe et  
127 al., 2024). The observed trend over this shorter period features a striking zonal temper-  
128 ature dipole, western Pacific warming and the eastern Pacific cooling, within the top 200m.  
129 This temperature dipole dynamically agrees with the upper ocean circulation strength-  
130 ening noted by Tuchen et al. (2024) over the overlapping period of 1993-2022.

131 In a series of recent studies inspired by Seager et al. (2019)'s hypothesis that the  
132 models' mean state ocean is simply too biased to capture observed SST trends, Jiang  
133 et al. (2024a, 2024b, 2025) highlight the differences in the subsurface trend patterns be-  
134 tween observations and models. In particular, the authors hypothesize that the observed  
135 subsurface cooling response can be explained as a forced response to wind changes (Jiang  
136 et al., 2024a, 2024b) and that models lack an effective connectivity between subsurface  
137 and surface eastern Pacific temperatures due to insufficient upwelling and mixing (Jiang  
138 et al., 2025). However, the corresponding 1958-2020 subsurface temperature trend com-  
139 posite from a suite of 11 large ensemble simulations from the sixth coupled model inter-  
140 comparison project [Figure 1b, inspired by Jiang et al. (2025)] shows a similar pattern  
141 to observations (Figure 1a; Pearson pattern correlation of 0.83). Both show a broad ther-  
142 mocline cooling, a somewhat zonally symmetric surface warming, and a sub-thermocline  
143 eastern Pacific warming. Despite model biases, the relative similarity between Figures  
144 1a and b suggest that the modeled subsurface temperature trend may still inform our  
145 understanding of the observed subsurface temperature trend and the coupled dynam-

146 ics that have created it. This perspective motivates the central questions of our study:  
147 1) which ocean dynamics contribute to this common modeled response, and 2) to what  
148 extent is the full response a simple linear combination of these responses?

149 A handful of studies have explored the models' shared central-western Pacific ther-  
150 mocline cooling response (c.f. Figure 1b and Figure S2) which has persisted for several  
151 model generations. Vecchi and Soden (2007) suggest that this cooling is a local effect  
152 caused by a reduction in thermocline tilt due to a weaker atmospheric Walker circula-  
153 tion. Yang et al. (2009) suggest that this weaker Walker circulation slows down the STCs  
154 and dynamically cools the equatorial subsurface. Luo et al. (2009, 2018) agree that mod-  
155 els' STCs have slowed, but suggest that a major cause of the slowdown is increased sub-  
156 tropical surface stratification. Finally, Ju et al. (2022) suggest that the cooling is caused  
157 by mean advection of density-compensated spiciness anomalies from the subtropics, which  
158 cool the region as much as dynamical changes in subtropical cell circulation.

159 While these studies provide a starting point for answering our guiding questions,  
160 it's evident that these proposed mechanisms are entwined with murky causality. A com-  
161 mon means of circumventing the attribution issues common to coupled dynamics is to  
162 employ a model hierarchy to step through a complex response by iteratively removing  
163 complexity until the phenomenon of interest is isolated. For instance, recent studies have  
164 overrode surface wind stress to mechanically decouple a GCM's ocean from its atmosphere  
165 (e.g., Luongo et al., 2024) and have shown that the ocean's full response to an anoma-  
166 lous forcing can be linearly partitioned into the response due to anomalous surface buoy-  
167 ancy forcing and anomalous surface momentum forcing (Luongo et al., 2022, 2023). Sim-  
168 ilarly, ocean-only GCM (OGCM) simulations are a convenient way to isolate just the ocean's  
169 response to a forcing without changes in the atmosphere (e.g., Peng et al., 2022).

170 In this study we employ a model hierarchy, consisting of a fully-coupled GCM, a  
171 mechanically-decoupled GCM, an OGCM, and a primitive equation reduced gravity model,  
172 to explore the modeled subsurface equatorial Pacific temperature response to greenhouse  
173 gas forcing and which ocean dynamics contribute to it. We discuss the simulations that  
174 comprise this hierarchy in section 2 and in section 3 we show that the full response can  
175 be understood as a linear sum of the response due to i) momentum effects, ii) remote  
176 buoyancy effects, and iii) local buoyancy effects. We discuss implications of these results  
177 in section 4 and we conclude in section 5.

178 **2 Model Hierarchy**

179 All simulations used to explore the equatorial Pacific thermocline response to green-  
 180 house gas forcing are presented in Table 1. Simulations that explore the equatorial Pa-  
 181 cific thermocline response to non-greenhouse-gas forcing schemes are presented in Ta-  
 182 ble S1.

Fully-coupled Simulations		
Simulation Name	CO <sub>2</sub> Forcing	Wind Stress
Ctrl	280ppm	Freely evolving
CO <sub>2</sub> x4	1120ppm	Freely evolving
Mechanically-decoupled Simulations		
Simulation Name	CO <sub>2</sub> Forcing	Wind Stress
Tau1CO <sub>2</sub> x1	280ppm	Ctrl
Tau1CO <sub>2</sub> x4	1120ppm	Ctrl
Tau4CO <sub>2</sub> x1	280ppm	CO <sub>2</sub> x4
Ocean-only Simulations		
Simulation Name	SST Forcing Perturbation	SST Forcing Bounds
Octrl	n/a	n/a
CO <sub>2</sub> x4_BFsst	Tau1CO <sub>2</sub> x4-Tau1CO <sub>2</sub> x1	90°S-90°N
CO <sub>2</sub> x4_BFsstET	Tau1CO <sub>2</sub> x4-Tau1CO <sub>2</sub> x1	90°S-6°S, 6°N-90°N
CO <sub>2</sub> x4_BFsstEQ	Tau1CO <sub>2</sub> x4-Tau1CO <sub>2</sub> x1	10°S-10°N
NEPac2CWarm	+2°C	147°W-123°W, 22°N-32°N
Reduced Gravity Simulations		
Simulation Name	Reduced Gravity	
RGctrl	1x	
RGx2	2x	

**Table 1.** Details of the fully coupled, mechanically-decoupled, ocean-only, and reduced-gravity simulations used to study the equatorial Pacific thermocline response to greenhouse gas forcing. Table S1 presents simulations that explore alternate forcing schemes.

## 183 **2.1 Fully-Coupled Simulations**

184 We analyze pre-existing simulations using the National Center for Atmospheric Re-  
 185 search’s Community Earth System Model, Version 1.2 (CESM1: Hurrell et al., 2013) that  
 186 were initially presented in Luongo et al. (2022) and Taylor et al. (2025). These simula-  
 187 tions have a nominal horizontal resolution of  $2^\circ$  in the atmosphere and land components  
 188 and  $1^\circ$  in the ocean and sea ice components. They are run in a standard coupled con-  
 189 figuration with pre-industrial forcing (“B1850” compset) for fifty years.

190 Our preindustrial control (Ctrl) simulation extends directly from initialization with  
 191 no anomalous forcing applied. To idealize climate change we apply and maintain an abrupt  
 192 quadrupling of  $\text{CO}_2$  relative to pre-industrial levels ( $\text{CO}_2 \times 4$ ). While abrupt quadrupling  
 193 of  $\text{CO}_2$  is an obvious simplification compared to a more realistic time-evolving increase  
 194 in  $\text{CO}_2$ , we show in section 3.1 that this idealization works remarkably well. While we  
 195 primarily focus on the equatorial Pacific’s response to greenhouse gas forcing in this study,  
 196 we also consider simulations with hemispherically asymmetric forcing to test how robust  
 197 the ocean dynamics of interest are to forcing geometry. We apply a zonally-uniform top-  
 198 of-atmosphere (TOA) insolation reduction following the Extratropical-Tropical Interac-  
 199 tion Model Intercomparison Project (ETINMIP: Kang et al., 2019) protocol in the North-  
 200 ern Hemisphere (NH,  $45^\circ\text{N}$ - $65^\circ\text{N}$ ) for ETINMIPNH and in the Southern Hemisphere (SH,  
 201  $45^\circ\text{S}$ - $65^\circ\text{S}$ ) for ETINMIPSH. The ETINMIP forcing corresponds to an annual-mean, zonal-  
 202 mean forcing of approximately  $-45 \text{ Wm}^{-2}$  at  $55^\circ$  N or S and falls off as an approximate  
 203 Gaussian. For all CESM1 simulations we consider an average over years 11-50 after the  
 204 forcing is applied as in Luongo et al. (2022, 2023).

## 205 **2.2 Mechanically-Decoupled Simulations**

206 We perform wind stress overriding simulations (e.g., Luongo et al., 2024) to iso-  
 207 late the dynamic effect of buoyancy and momentum flux anomalies on the ocean, while  
 208 still maintaining some amount of realistic atmosphere-ocean coupling. In a fully-coupled  
 209 simulation the coupler interactively provides the ocean component with atmospheric wind  
 210 stress. This momentum flux hand-off then drives changes in the ocean state (e.g., equa-  
 211 torial thermocline tilt which changes the zonal SST gradient), which can then feed back  
 212 on the atmosphere in the next coupling step (e.g., Bjerknes feedback). In wind stress over-  
 213 riding simulations, however, the GCM is instead modified to receive a known surface wind

214 stress field, disabling the interactive hand-off of momentum fluxes and mechanically de-  
 215 coupling the ocean from the atmosphere. All other coupling, including the effect of wind  
 216 speed on turbulent heat fluxes, remain in tact.

217 In our mechanically-decoupled simulations we either apply a radiative forcing ( $\text{CO}_2$   
 218 quadrupling or ETINMIP TOA forcing) and lock to Ctrl’s wind stress field, or we ap-  
 219 ply no radiative forcing but we lock to a perturbed simulation’s wind stress field. For  
 220 example, we perform a simulation where we abruptly quadruple  $\text{CO}_2$ , but we override  
 221 with unperturbed Ctrl wind stress (Tau1CO<sub>2</sub>x4). This simulation highlights the radiatively-  
 222 driven climate response because wind stress is unperturbed. We also perform a simu-  
 223 lation where we apply no  $\text{CO}_2$  forcing, but we override with the perturbed wind stress  
 224 field from CO<sub>2</sub>x4 to highlight the climate response just due to wind stress (Tau4CO<sub>2</sub>x1).  
 225 Similarly, we perform a simulation where we apply a reduction in insolation in the NH  
 226 following the ETINMIP protocol described above, but we override with unperturbed Ctrl  
 227 wind stress (Tau1SNH), and we perform a simulation where we apply no insolation re-  
 228 duction, but we override with the perturbed wind stress field from ETINMIPNH (TauNHS1).  
 229 Tau1SSH and TauSHS1 are similar, but correspond to the SH ETINMIP simulations.

230 In these wind overriding simulations we prescribe the full interannually-varying wind  
 231 stress field to maintain the impact of high-frequency mechanical variability on the sur-  
 232 face ocean and reduce mean state biases (Luongo et al., 2024). Finally, in order to only  
 233 compare mechanically-decoupled simulation to mechanically-decoupled simulation and  
 234 subtract out remaining mean state biases, we compare these perturbed mechanically-decoupled  
 235 simulations to a control mechanically-decoupled simulation (Tau1CO<sub>2</sub>x1), which has no  
 236 radiative forcing and wind stress locked to Ctrl. As such, our buoyancy-forced (BF) re-  
 237 sponse is Tau1CO<sub>2</sub>x4-Tau1CO<sub>2</sub>x1 and our momentum-forced (MF) response is Tau4CO<sub>2</sub>x1-  
 238 Tau1CO<sub>2</sub>x1. See discussion in Luongo et al. (2022, 2023, 2024) for more detail on this  
 239 protocol.

### 240 **2.3 Ocean-only Simulations**

241 We use an ocean-only version of the Massachusetts Institute of Technology Gen-  
 242 eral Circulation Model (MITgcm) in the same configuration used in Luongo et al. (2025),  
 243 which is similar to the Estimated the Circulation and Climate of the Ocean version 4  
 244 release 4 (ECCOv4r4: Forget et al., 2015) configuration. This OGCM has 1° horizon-  
 245 tal resolution in the zonal direction and 1/3° meridional resolution at high and low lat-

246 itudes (telescoping to  $1^\circ$  in midlatitudes). While not fully permitting high latitude mesoscale  
 247 eddies, the higher resolution in the equatorial region begins to resolve equatorial waves  
 248 and thus decrease tropical biases. This MITgcm configuration is forced with monthly  
 249 climatologies of net air-sea fluxes of heat, freshwater, shortwave radiation, and zonal and  
 250 meridional momentum diagnosed by Peng et al. (2022) from a 25-year control integra-  
 251 tion of ECCOv4r4 with bulk formulae forcing. In addition to climatological flux forc-  
 252 ing, we restore SST and sea surface salinity to Peng et al. (2022)’s climatologies on a 10-  
 253 day timescale. All of our OGCM simulations branch from a 100-year spin-up, at which  
 254 point the upper-ocean is approximately equilibrated. See Luongo et al. (2025) for fur-  
 255 ther details.

256 Our OGCM control simulation (OCtrl) is integrated for 30 years. We also perform  
 257 a series of perturbation experiments where we add the anomalies in the buoyancy-forced  
 258 (BF) SST field diagnosed from our mechanically-decoupled CESM1 simulations to the  
 259 SST relaxation field. We add anomalies in the quasi-equilibrium (average over years 11-  
 260 50) SST field calculated from Tau1CO<sub>2</sub>x4-Tau1CO<sub>2</sub>x1, Tau1SNH-Tau1CO<sub>2</sub>x1, and Tau1SSH-  
 261 Tau1CO<sub>2</sub>x1 (producing ocean-only simulations CO<sub>2</sub>x4\_BFsst, ETINMIPNH\_BFsst, and  
 262 ETINMIPSH\_BFsst, respectively). Comparing these SST-forced perturbation experiments  
 263 with OCtrl shows the ocean-only dynamic response to the buoyancy-driven SST response.

264 Finally, we split these perturbation experiments geographically into SST forcing  
 265 from only the extratropical regions and SST forcing from only the equatorial region (“ET”  
 266 or “EQ” appended to above names). In the extratropical SST forcing experiment we ap-  
 267 ply the full CESM1 buoyancy-driven SST anomaly field from  $90^\circ\text{S}$ - $11^\circ\text{S}$  and  $11^\circ\text{N}$ - $90^\circ\text{N}$ .  
 268 We linearly taper this forcing to zero over  $5^\circ$  to  $6^\circ\text{S}$  and  $6^\circ\text{N}$  to avoid artificially large  
 269 meridional forcing gradients. There is no anomalous SST forcing from  $5^\circ\text{S}$ - $5^\circ\text{N}$  in the  
 270 extratropical SST forcing experiment. Similarly, in the equatorial SST forcing experi-  
 271 ment we apply the full CESM1 buoyancy-driven SST anomaly field from  $5^\circ\text{S}$ - $5^\circ\text{N}$ , cre-  
 272 ate a  $5^\circ$  linear taper to  $10^\circ\text{S}$  and  $10^\circ\text{N}$ , and do not anomalously force SST anywhere else.  
 273 While we somewhat arbitrarily chose these meridional boundaries, we have found that  
 274 using  $10^\circ\text{S}$  and  $10^\circ\text{N}$  for the full forcing bounds of the equatorial SST forced simulation  
 275 (and changing other bounds accordingly) leads to small differences that do not affect our  
 276 conclusions (not shown). For all OGCM simulations we consider the average over years  
 277 11-30 after the forcing is applied as in Luongo et al. (2025).

## 2.4 Reduced Gravity Simulations

Finally, we run two simulations using the 1.5-layer reduced gravity (RG) model from Sun and Thompson (2020) to represent an idealization of the upper branch of the global overturning circulation’s response to an increase in surface stratification. The model’s geography consists of three idealized ocean basins representing the Atlantic, Indian, and Pacific oceans and a zonally re-entrant channel representing the Southern Ocean from 45°S to the southern boundary. The total width is 220° and the latitudinal extent is from 72°S-72°N. The model solves for upper layer thickness, approximating thermocline depth, and is solved on a B-grid with 1° horizontal spacing. Surface water mass transformation in the Southern Ocean is represented as a relaxation of upper layer thickness to 10m near the southern boundary, and North Atlantic Deep Water formation is represented as a constant downwelling velocity in the North Atlantic. Sun and Thompson (2020) provide further details on this model.

We run two reduced gravity simulations. The first is a control simulation using standard parameters from Sun and Thompson (2020) (RGCtrl). The second branches from the tenth year of RGCtrl and instantaneously doubles the reduced gravity parameter RG to represent a stratification increase in response to climate change forcing (RGx2). We compare the difference between these two simulations ten years after that branch point.

## 3 Results

### 3.1 Buoyancy and Momentum Dynamics Create the Full Response

Despite the fact that our CESM1 simulations idealize climate change as an abrupt and continuous quadrupling of CO<sub>2</sub>, the upper-ocean quasi-steady fully-coupled (FC) response (Figure 2a) bears a striking resemblance to the multi-ensemble mean response to realistic historical forcing in Figure 1b (Pearson pattern correlation of 0.94). As in the multi-model response, the FC equatorial temperature response features a thermocline cooling in the central Pacific, a strong surface warming that is deeper in the western Pacific than the eastern Pacific, and a sub-thermocline warming in the eastern Pacific. Luo et al. (2018) show a very similar CESM1 response to abrupt quadrupling of CO<sub>2</sub> (over years 41-90), which in turn also resembles the transient response (years 1-10) to this same forcing in two prior versions of CESM (Heede et al., 2021). It is interesting that the equatorial Pacific’s subsurface temperature response to abrupt idealized cli-

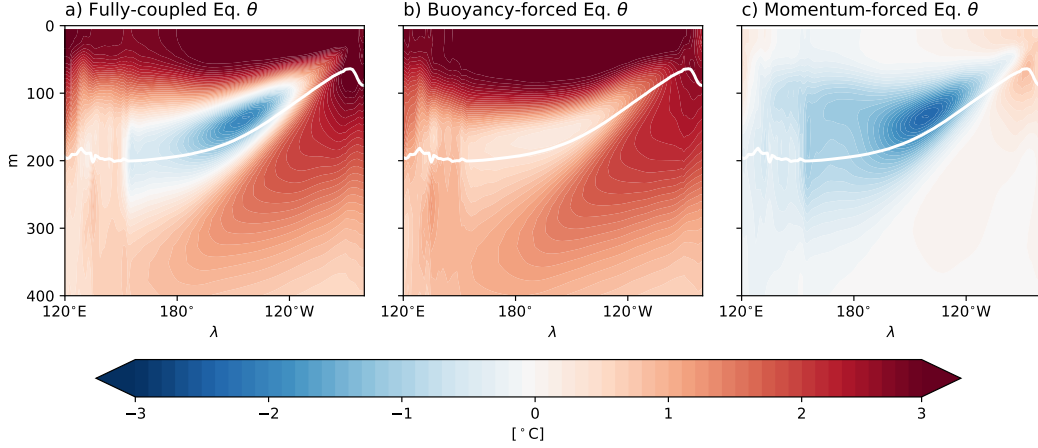


**Figure 2.** a) CESM1 fully-coupled (FC = CO<sub>2</sub>x4-Ctrl) equatorial temperature ( $\theta$ ) response to abrupt quadrupling of CO<sub>2</sub>. b) CESM1 buoyancy-forced (BF = Tau1CO<sub>2</sub>x4-Tau1CO<sub>2</sub>x1) equatorial  $\theta$  response to abrupt quadrupling of CO<sub>2</sub>. c) CESM1 momentum-forced (MF = Tau4CO<sub>2</sub>x1-Tau1CO<sub>2</sub>x1) equatorial  $\theta$  response to abrupt quadrupling of CO<sub>2</sub>. All panels are meridionally averaged from 5°S-5°N, temporally averaged from years 11-50, and they show the 16°C isotherm from the Ctrl simulation as a white contour to approximate the thermocline.

309 mate change matches the response pattern to historical forcing so well, particularly since  
 310 this does not extend to SST (Wills et al., 2022). However, Heede et al. (2021) showed  
 311 that the prominent thermocline cooling response to abrupt quadrupling disappears af-  
 312 ter 200 years and is instead replaced by a near-zero temperature response. While the cen-  
 313 tennial response to abrupt 4xCO<sub>2</sub> forcing is an unrealistic analog for transient climate  
 314 change, the multi-decadal response to abrupt 4xCO<sub>2</sub> forcing shown in Figure 2a appears  
 315 to be an appropriate tool for studying the multi-model response to historical forcing.

316 As in Luongo et al. (2023), who instead consider the subsurface equatorial temper-  
 317 ature response to NH ETINMIP forcing, we find that the FC equatorial temperature re-  
 318 sponse to CO<sub>2</sub> forcing (Figure 2a) is highly linear. That is, the fully-coupled (FC) re-  
 319 sponse to CO<sub>2</sub> forcing can be neatly linearly decomposed into the buoyancy-forced (BF)  
 320 response (Figure 2b) and the momentum-forced (MF) response (Figure 2c):

$$\text{FC} \approx \text{BF} + \text{MF} . \quad (1)$$

321 These patterns closely resemble the FC, BF, and MF responses to NH ETINMIP forc-  
322 ing (but with opposite sign because ETINMIP forcing is a cooling) presented in Luongo  
323 et al. (2023) and recreated in Figures S3a-c. This resemblance is also found in response  
324 to SH ETINMIP forcing (Figure S3d-f). This similarity between equatorial temperature  
325 responses was not expected a priori because abrupt 4xCO<sub>2</sub> is a nearly hemispherically  
326 symmetric forcing while ETINMIP forcing is purposefully hemispherically asymmetric.  
327 We discuss this further in Section 4.

328 The MF response, created by momentum-driven dynamics, is the cause of the promi-  
329 nent thermocline cooling seen in the FC response. This cooling is maximized within the  
330 thermocline and is a major feature across the majority of the basin. However, while weak  
331 cooling extends from surface to depth in the western Pacific, even the strong cooling in  
332 the thermocline dissipates before reaching the eastern boundary. Instead the eastern equa-  
333 torial Pacific from the surface to below the thermocline features weak warming. This zonal  
334 temperature dipole is a feature of relaxed thermocline tilt: a shoaling of the western Pa-  
335 cific thermocline and a deepening of the eastern Pacific thermocline would respectively  
336 manifest as a cooling and warming in depth space. The relaxed thermocline tilt in FC,  
337 caused by westerly anomalies in equatorial wind stress from a weakened Walker Circu-  
338 lation (not shown), agrees with Vecchi and Soden (2007)'s hypothesis that the thermo-  
339 cline cooling response to climate change results from a decadal Bjerknes-like response  
340 to relaxed wind stress. Similarly, it qualitatively agrees with Jiang et al. (2024b, 2025)'s  
341 assertion that winds have driven much of the observed subsurface equatorial tempera-  
342 ture response. We note, however, that because the MF response does not include greenhouse-  
343 gas-driven increases in subtropical stratification and yet it accounts for all FC thermo-  
344 cline cooling, that this understanding disagrees with the arguments proposed by Luo et  
345 al. (2009, 2018) and Ju et al. (2022) that increased subtropical stratification creates this  
346 cooling by either slowing the STCs or advecting density-compensated anomalies.

347 Perhaps unsurprisingly, the BF response, which captures the ocean's response to  
348 anomalous buoyancy fluxes from increased CO<sub>2</sub> radiative forcing, contributes nearly all  
349 of the warming seen in FC. This includes a strong surface warming maximized in the cen-  
350 tral Pacific and most of the eastern Pacific's sub-thermocline warming. Interestingly, the  
351 central Pacific thermocline region in BF has a near-zero temperature response in the ex-  
352 act same region where MF cools. This allows the relatively strong momentum-driven cool-  
353 ing to clearly establish itself in FC. The near-zero temperature response of the BF ther-

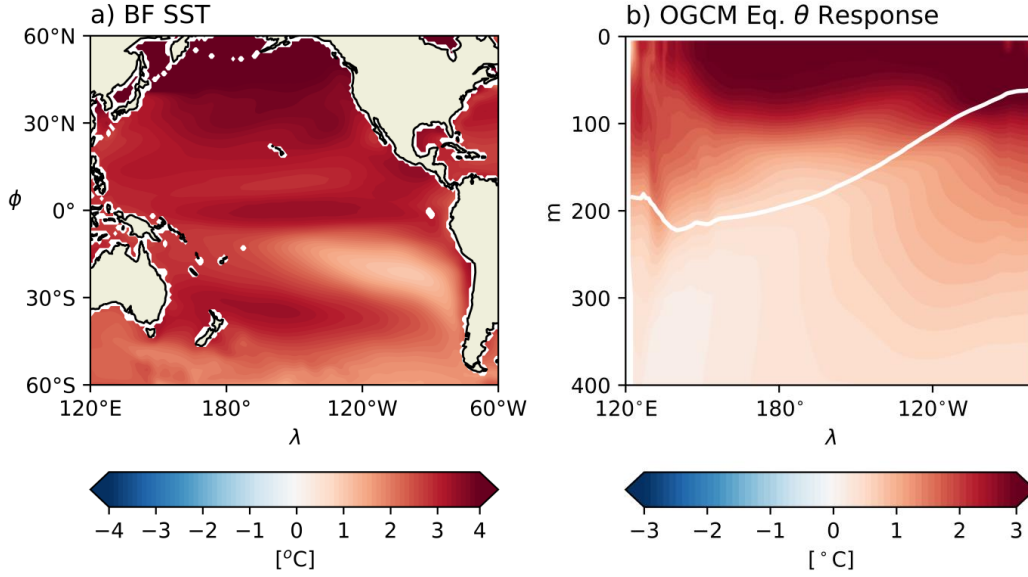


**Figure 3.** a) Buoyancy-forced quasi-steady (year 11-50) SST response in CESM1. b) MITgcm equatorial temperature ( $\theta$ ) response to SST forcing in panel a) averaged over years 11-30.

354 mocline, which strongly resembles the full centennial response to abrupt forcing seen in  
 355 Heede et al. (2021), also implies a relatively long-lasting upwelling damping effect. This  
 356 calls into question the conventional understanding of the the ocean dynamical thermo-  
 357 stat as a transient phenomenon (e.g., Luo et al., 2017; Heede et al., 2020; Heede & Fe-  
 358 dorov, 2021).

359 This BF pattern, with its near-zero thermocline response, strong surface warming,  
 360 and sloping sub-thermocline eastern Pacific warming, is not obviously attributable to well-  
 361 known dynamics. Both conventional advective (ocean-tunnel) and dynamical (wave-driven)  
 362 understandings of the STCs instead suggest broad thermocline warming. While Luongo  
 363 et al. (2023) perform an ocean mixed layer heat decomposition on the equatorial SST  
 364 response to NH ETINMIP forcing and attribute a certain amount of the BF SST response  
 365 to ocean dynamics, the specific dynamic adjustments remain unclear. As such, we turn  
 366 to MITgcm ocean-only simulations to explain the ocean dynamics that create the sub-  
 367 surface BF response to climate change forcing seen in Figure 2b.

### 368 **3.2 Recreating the Buoyancy Response**

369 To determine whether MITgcm is an appropriate tool with which to understand  
 370 the ocean dynamics that create the buoyancy-driven mechanically-decoupled CESM1 re-  
 371 sponse in Figure 2b, we first test whether MITgcm is able to effectively recreate CESM1’s  
 372 response at all. In the CO<sub>2</sub>x4\_BFsst OGCM simulation we add the global quasi-steady  
 373 buoyancy-forced SST response to abrupt 4xCO<sub>2</sub> forcing (Figure 3a) to MITgcm’s monthly  
 374 climatological SST relaxation fields. Because we do not change any other forcing fields,  
 375 the difference between this simulation and OCtrl is the ocean-only response to that SST  
 376 forcing pattern.

377 MITgcm does a surprisingly good job of recreating the major features of CESM1’s  
 378 quasi-steady buoyancy-forced subsurface equatorial temperature response (c.f. Figures  
 379 2b and 3b, Pearson pattern correlation of 0.86). The MITgcm temperature response fea-  
 380 tures the strong, relatively zonally symmetric near-surface warming, a warming mini-  
 381 mum in the central-western Pacific thermocline, and sloping sub-thermocline warming  
 382 in the eastern Pacific. There are some notable differences between the two patterns, most  
 383 obviously that the near-zero thermocline warming so obvious in CESM1 is deeper, more  
 384 westward, and more diffuse in MITgcm. The eastern Pacific sub-thermocline warming  
 385 is also weaker in MITgcm. However, MITgcm and CESM1 are entirely different ocean  
 386 models with entirely different mean states, parameterizations, and resolution. Given this  
 387 reality, we consider the otherwise substantial agreement between Figures 2b and 3b to  
 388 be promising, and we conclude that these ocean-only simulations are a reasonable diag-  
 389 nostic tool for understanding mechanically-decoupled simulations.

390 Having shown that the MITgcm response to the full BF SST field reasonably recre-  
 391 ates the CESM1 response, we now ask whether we can decompose this full response fur-  
 392 ther, namely into the response to SST forcing from different geographic regions. This  
 393 question emerges directly from the canonical advective ocean tunnel understanding of  
 394 the non-wind-driven STC response to climate change (e.g., Clement et al., 1996; Luo et  
 395 al., 2009, 2017, 2018; Heede & Fedorov, 2021; Ju et al., 2022), which suggests that warm  
 396 subtropical surface waters subduct in the eastern half of the subtropical gyre, are car-  
 397 ried by mean advection to the western boundary, penetrate into the tropics via low lat-  
 398 itude western boundary currents, and eventually warm the thermocline. Because this  
 399 understanding suggests that some portion of the equatorial temperature response is en-

400 tirely remotely-driven, we run two OGCM simulations to determine whether we can un-  
 401 derstand the full response to BF SST forcing as the sum of patterns created by remote  
 402 and local SST forcing. We do this by regionally partitioning the full BF SST forcing field  
 403 in Figure 3a into remote extratropical (ET: Figure 4a) and local equatorial (EQ: Fig-  
 404 ure 4b) SST forcing fields.

405 The sum of the remote (Figure 4c) and local (Figure 4d) responses almost perfectly  
 406 recreates the full field response in Figure 3b (not shown, Pearson pattern correlation of  
 407 0.98). However, while these patterns sum to the full response, they differ substantially  
 408 and clearly represent different oceanic dynamics. We explore the ocean adjustments that  
 409 create the remote and local response in the following two subsections.

### 410 ***3.2.1 Adjustments to Remote Buoyancy Forcing***

411 We first consider the equatorial temperature response to extratropical-only BF SST  
 412 forcing (Figure 4c). The equatorial Pacific subsurface warms in response to this remote  
 413 forcing, with no evidence of cooling. The warming is maximized within the thermocline  
 414 throughout the entire basin. Despite strong surface relaxation to unperturbed SSTs, the  
 415 strong near-surface thermocline warming in the eastern equatorial Pacific extends to the  
 416 surface. In addition, it is clear that the sloping sub-thermocline warming in the eastern  
 417 Pacific noted in the FC and BF CESM1 responses above is caused by this remote ad-  
 418 justment.

419 This coherent warming of the equatorial thermocline in response to remote SST  
 420 forcing in both hemispheres is strikingly similar to the equatorial temperature response  
 421 to a  $+2^{\circ}\text{C}$  SST anomaly in the northeast Pacific stratocumulus deck as presented in Luongo  
 422 et al. (2025)'s NEPac2CWarm simulation (c.f. Figures 4c and 5b, Pearson pattern cor-  
 423 relation of 0.94). In that study we used MITgcm to investigate how the tropical ocean  
 424 responded to subtropical surface cooling. We showed that both circulation adjustments  
 425 ( $v'\bar{\theta}$ ) and mean advection of temperature anomalies ( $\bar{v}\theta'$ ) communicated subtropical cool-  
 426 ing to the tropics within about a decade. At the equator, an equatorial Kelvin wave co-  
 427 herently heaved the thermocline as it traveled eastward. Upon hitting the eastern bound-  
 428 ary, this wave signal radiated poleward in both hemispheres as coastal Kelvin waves, which  
 429 then proceed to adjust stratification in the eastern basin by shedding westward-propagating  
 430 Rossby waves. Although we primarily focused on subtropical cooling in Luongo et al.

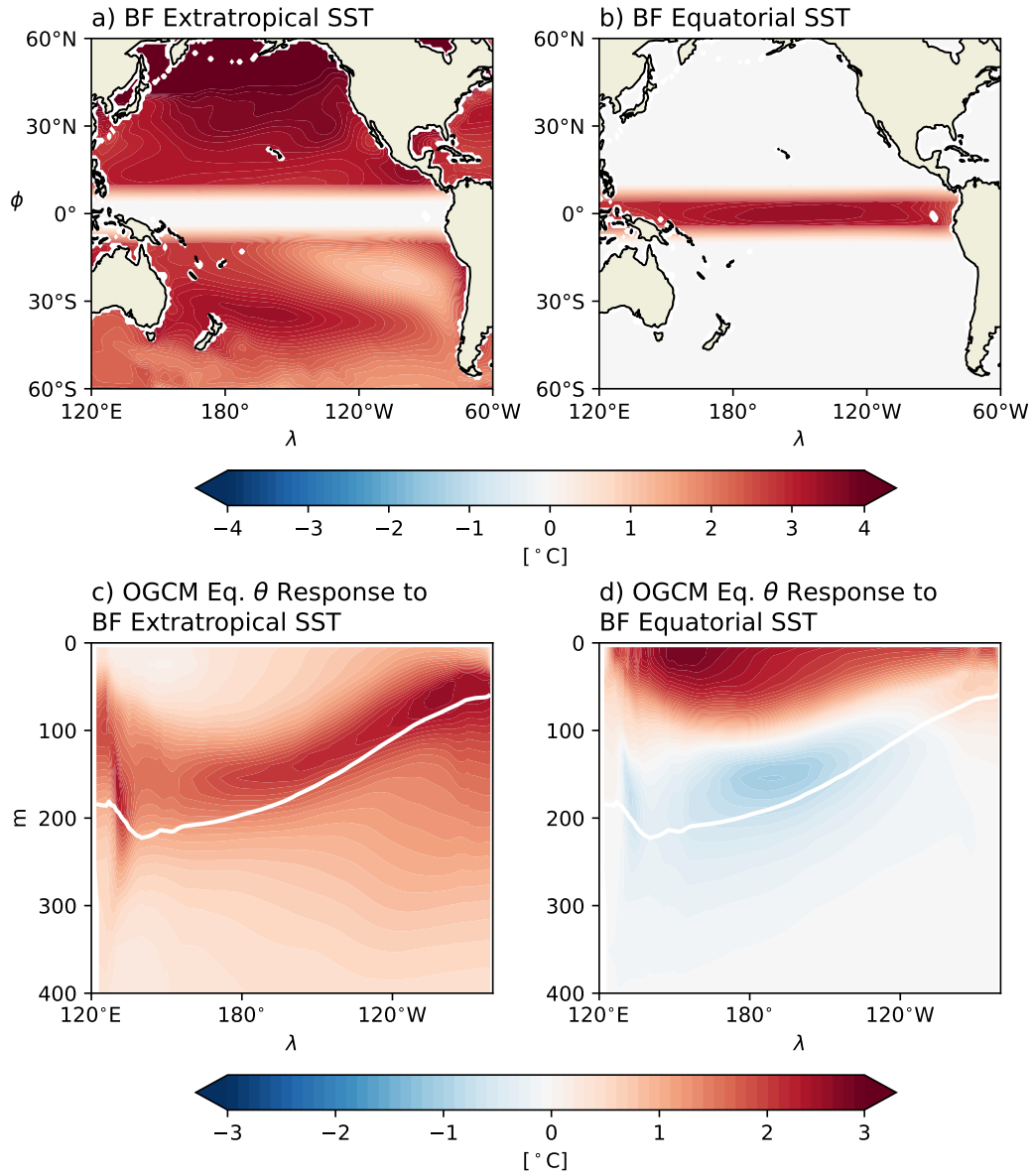


**Figure 4.** a) Remote, extratropical component of BF SST response in Figure 3a. b) Local, equatorial component of BF SST response in Figure 3a. c) Equatorial  $\theta$  response to remote SST forcing in panel a). d) Equatorial  $\theta$  response to local SST forcing in panel b).

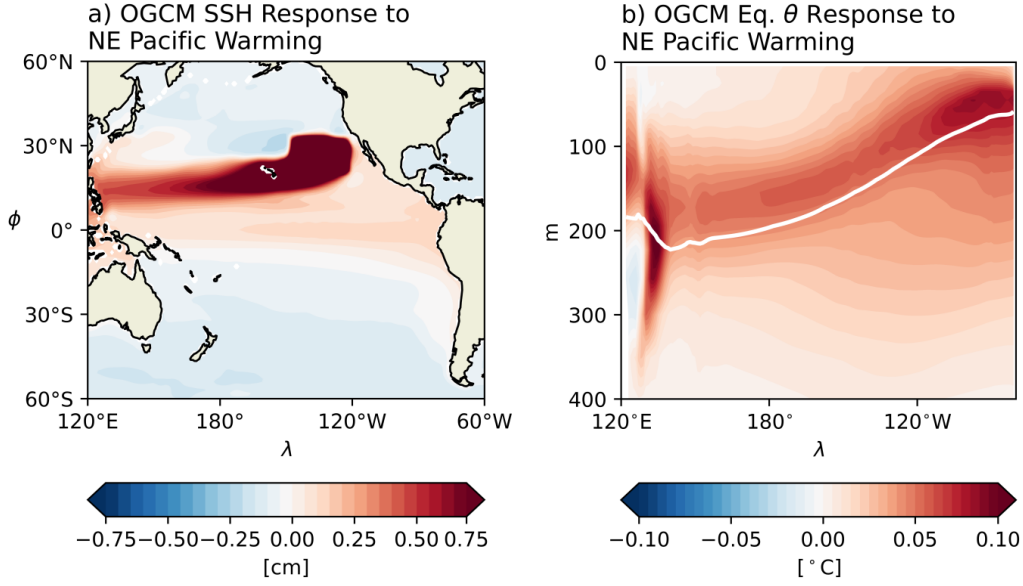


**Figure 5.** a) Sea surface height (SSH) response to NEPac2CWarm simulation from Luongo et al. (2025). b) Equatorial  $\theta$  response to NEPac2CWarm simulation.

431 (2025), the NEPac2CWarm response presented in Figure 5 demonstrates that the equa-  
 432 torial temperature response to subtropical warming is simply the opposite of its response  
 433 to subtropical cooling. It is also relevant to note that Luongo et al. (2025) showed that  
 434 both NH and SH subtropical forcing led to similar equatorial response patterns due to  
 435 the symmetric nature of the equatorial Kelvin wave adjustment.

436 In the case of CO<sub>2</sub>x4.BFsstET, the dynamics clarified in Luongo et al. (2025) sug-  
 437 gest that strong subtropical warming present in both NH and SH (Figure 4a) contribute  
 438 to the warming of the equatorial thermocline (Figure 4c). This warming occurs through  
 439 both mean advection of warm anomalies, as in the canonical ocean tunnel understand-  
 440 ing, but also due to the coherent deepening of the equatorial thermocline via a down-  
 441 welling Kelvin wave excited by the subtropical gyres' baroclinic response to anomalous  
 442 surface warming. This dynamical adjustment is in-turn responsible for the eastern Pa-  
 443 cific's sloping sub-thermocline warming, a slow stratification adjustment to the heaved  
 444 thermocline. As such, we re-emphasize the importance of the STC as a dynamic mech-  
 445 anism to communicate subtropical warming to the equatorial thermocline.

446

### 3.2.2 Adjustments to Local Buoyancy Forcing

447

448

449

450

451

452

453

454

455

456

The response of the subsurface equatorial Pacific to the local buoyancy-forced component of climate change forcing (Figure 4d) unsurprisingly features strong near-surface warming which is directly tied to the applied tropical SST forcing (Figure 4b). However, perhaps unexpectedly, the local response features substantial cooling across much of the thermocline that underlies the strong near-surface warming. In the western Pacific, where the mean thermocline and anomalous near-surface warming signal are deepest, this thermocline cooling response extends from approximately 100-400m. As the mean thermocline tilts upward to the east, this cooling signal gets shallower and thinner until the temperature anomaly switches signs to warming around 110°W. The thermocline then remains anomalously warm all the way to the eastern boundary.

457

458

459

460

461

462

463

464

465

466

467

Luo et al. (2018) used an OGCM to explore the response of the equatorial thermocline to a uniform tropical warming of 3.2°C. They find a pattern of near-surface warming and thermocline cooling that is similar to our response to local BF. In that work, Luo et al. (2018) suggested that this temperature response was a local baroclinic adjustment to surface warming: as near-surface stratification increases in response to surface warming, turbulent downward mixing of that heat decreases and creates a cooling signal (Yang et al., 2009). Luo et al. (2018), therefore, would attribute much of the cooling in Figure 4d to be a signal of reduced mixing. We note, however, that this mechanism does not explain the zonal temperature dipole clearly seen in our thermocline response to local BF: as discussed above, a zonal dipole instead implies a thermocline tilt and suggests the need to consider zonal gradients.

468

469

470

471

472

473

474

475

To determine whether the local response can instead be understood in terms of inviscid dynamics, we model the equatorial ocean as a simple 1.5-layer reduced gravity system. In this simplified understanding, the lower level flow is negligible compared to upper level flow ( $\vec{u}_1, \vec{v}_1 \gg \vec{u}_2, \vec{v}_2 = 0$ ), the layers are coupled by their density differences via the reduced gravity parameter [ $g' \equiv g(\rho_2 - \rho_1)/\rho_2$ ], and the interface depth,  $h = \eta + H$ , is thermocline depth defined positive downward and as a sum of interface displacement  $\eta$  and mean thermocline depth  $H$ . Ignoring dissipation terms, the steady, linear equatorial zonal momentum equation in conservative flux form is

$$0 = -\left(g' \frac{h^2}{2}\right)_x + \frac{\tau^x}{\rho_0}, \quad (2)$$

476 where  $\tau^x$  is zonal wind stress,  $\rho_0$  is a constant reference density, and the  $x$  subscript rep-  
 477 represents a zonal derivative. If we now instead consider the non-conservative velocity form  
 478 of Equation 2 linearized about  $H$ ,

$$0 = -g' \eta_x + \frac{\tau^x}{\rho_0 H}, \quad (3)$$

479 and we consider a  $\Delta$  climate change forcing without changes in  $\tau^x$  (as is the case in our  
 480 OGCM simulations), the balance becomes

$$\Delta g' \overline{\eta_x} = -\overline{g'} \Delta \eta_x. \quad (4)$$

481 Equation 4 demonstrates, without making any assumptions about the eastern bound-  
 482 ary, that the product of the perturbed RG and the mean zonal gradient of interface dis-  
 483 placement must be balanced by the product of the mean RG and a perturbed zonal gra-  
 484 dient of interface displacement. In the case of climate change driven warming, because  
 485  $\Delta g' > 0$  we expect  $\Delta \eta_x > 0$ . Put another way, an increase in stratification should re-  
 486 duce the tilt of the thermocline even with no change in winds, in turn leading to west-  
 487 ern thermocline cooling and eastern thermocline warming.

488 We test this tilt hypothesis with two simulations using Sun and Thompson (2020)'s  
 489 idealized global ocean reduced gravity model (Figure 6a), comparing a simulation where  
 490 the reduced gravity parameter is doubled (RGx2) to one where it isn't (RGCtrl). Fig-  
 491 ure 6b shows the  $\eta$  response in the equatorial Pacific 10 years after RG is doubled. We  
 492 see that the western equatorial Pacific interface displacement decreases (shoals), while  
 493 the eastern equatorial Pacific interface displacement increases (deepens). This western  
 494 Pacific shoaling and eastern Pacific deepening corresponds to a relaxation in thermocline  
 495 tilt, or a western thermocline cooling and an eastern thermocline warming. We use this  
 496 newly gained physical intuition to explain the thermocline temperature dipole in Fig-  
 497 ure 4d, which then adds to the coherent thermocline shoaling pointed out by Luo et al.  
 498 (2018). While this coherent shoaling response could theoretically be due to mixing, if  
 499 we make the assumption that the eastern boundary interface depth in Equation 4 is ap-  
 500 proximately fixed, then this inviscid balance leads to thermocline shoaling that increases  
 501 westward.

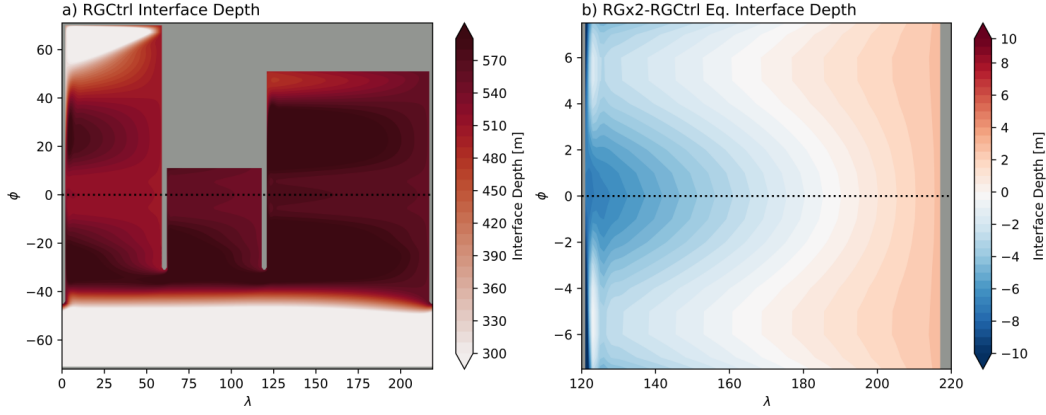


**Figure 6.** a) Interface depth in idealized global RG model after 20 years of spin-up in RGCtrl. b) Equatorial interface depth response to RGx2-RGCtrl’s doubling of reduced gravity at year 10.

502 In summary, we conclude that the local response of the equatorial thermocline to  
 503 the equatorial buoyancy-driven SST response to climate change consists of two responses  
 504 to the increase in near-surface stratification: both a coherent thermocline shoaling and  
 505 a decrease in thermocline tilt. This latter point questions the oft-held view that a tilted  
 506 thermocline is necessarily tied to a change in zonal winds.

## 507 4 Discussion

### 508 4.1 Linearity of the Equatorial Thermocline’s Response

509 We use a hierarchy of models to show that the full subsurface temperature response  
 510 of the equatorial thermocline to greenhouse gas forcing ( $\theta_{FC}$ : Figure 2a) can be recov-  
 511 ered as a relatively simple linear combination of independent ocean dynamical responses.  
 512 As in Luongo et al. (2023), we use a mechanically decoupled model to show that  $\theta_{FC}$   
 513 is the sum of the wind stress-driven response ( $\theta_{MF}$ : Figure 2c) and the buoyancy-driven  
 514 response ( $\theta_{BF}$ : Figure 2b). We then use OGCM simulations to show that  $\theta_{BF}$  can be  
 515 linearly partitioned into a sum of forced responses from different geographic regions of  
 516 SST forcing: a remote, extratropically-driven response ( $\theta_{BF,remote}$ : Figure 4c) and a lo-  
 517 cal, equatorially-driven response ( $\theta_{BF,local}$ : Figure 4d). The remote response represents  
 518 the dynamically and thermodynamically-driven changes of the thermocline in response  
 519 to subtropical temperature forcing, as outlined in Luongo et al. (2025). We then use a  
 520 RG model to show that the local response is consistent with a response to surface strat-

521 ification that includes both shoaling and reduced thermocline tilt. Putting this all to-  
 522 gether, we present this linear understanding as

$$\begin{aligned} \theta_{FC} &= \theta_{MF} + \theta_{BF} = \theta_{MF} + \theta_{BF,remote} + \theta_{BF,local} \\ &= \alpha * MF(\tau^x, \tau^y) + \beta * BF_{remote}(NH\ SST, SH\ SST) + \gamma * BF_{local}(Eq.\ SST) . \end{aligned} \quad (5)$$

523 Equation 5 communicates that the full response of the modeled tropical Pacific sub-  
 524 surface temperature response to greenhouse gas forcing is a linear combination of ocean  
 525 dynamics driven by momentum from zonal and meridional wind stress, buoyancy from  
 526 NH and SH subtropical SST forcing, and buoyancy from local equatorial SST forcing,  
 527 with  $\alpha$ ,  $\beta$ , and  $\gamma$  as scaling coefficients. This is the primary result of our study. Because  
 528 our FC CESM1 response to abrupt quadrupling of CO<sub>2</sub> strongly resembles both the 1958-  
 529 2020 observed (Figure 1a) and multi-model mean (Figure 1b) response to realistic, his-  
 530 torical climate change forcing, we conclude that this simple linear understanding gained  
 531 from a hierarchy of idealized modeling simulations is a powerfully relevant and applica-  
 532 ble tool with which to understand realistic climate change.

533 While this understanding is simple at face value, it in fact suggests that the equa-  
 534 torial temperature response to even just steady, idealized greenhouse gas forcing is more  
 535 complex than previously understood. We see that the full response actually contains many  
 536 of the dynamics previously suggested in the literature (e.g. Clement et al., 1996; Sea-  
 537 ger & Murtugudde, 1997; Vecchi & Soden, 2007; Luo et al., 2009, 2018; Heede et al., 2020,  
 538 2021; Watanabe et al., 2024). Nevertheless, it is only through understanding the com-  
 539 bination of these dynamics that we can critically update our theoretical picture for how  
 540 the equatorial Pacific will respond to climate change.

## 541 4.2 Reconstructing Long and Short-Term Climate Change Responses

542 As suggested by Equation 5, we seek to reconstruct the observed equatorial sub-  
 543 surface temperature trends from 1958-2020 (Figure 1a) as a linear combination of the  
 544 MF and remote and local BF patterns. We use a depth-weighted ordinary least squares  
 545 multilinear regression to determine combination coefficients. Our reconstruction of the  
 546 1958-2020 trend (Figure 7a) shows strong agreement with the observational composite  
 547 (Figure 1a), with a Pearson pattern correlation of 0.86. We are able to explain much of  
 548 both the models' and observations' long-term subsurface temperature response through

549 our linear understanding of oceanic dynamics. Interestingly, we note that while the re-  
 550 gression coefficients for the MF and local BF responses are positive (meaning they are  
 551 in line with greenhouse gas forcing), the remote BF response is slightly negative (Fig-  
 552 ure 7c). This suggests that subtropical temperature forcing has not majorly impacted  
 553 the equatorial thermocline in this period, and, if it has, it's been a cooling signal. This  
 554 could hypothetically be due to a cooling trend in Southern Ocean surface temperatures  
 555 (e.g., Dong et al., 2022).

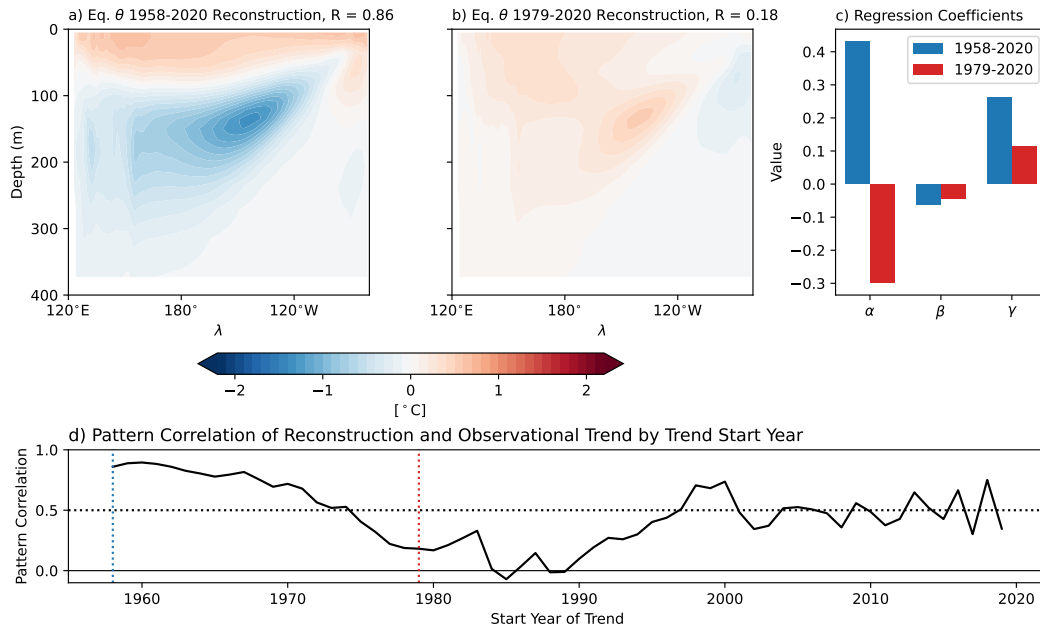


**Figure 7.** a) 1958-2020 reconstruction of Figure 1a observational trend using  $\alpha$ \*MF pattern +  $\beta$ \*remote BF pattern +  $\gamma$ \*local BF pattern. b) As in a), but for 1979-2020 observational trend of Figure 1c. c) Regression coefficients for linear combinations in a) and b). d) Pearson pattern correlation between regression-estimated reconstruction and observed trend as a function of trend start year. The dotted blue line highlights 1958, the dotted red line highlights 1979, and the dotted black line is at a correlation value of 0.5.

556 While the multi-model mean trend is obviously similar to the observed trend over  
 557 1958-2020, the observed 1979-2020 trend is notably distinct from the modeled trend over  
 558 that same period (c.f. Figure 1c & d). Indeed, our multilinear regression method can not  
 559 successfully reconstruct this more recent period's observed temperature trend (Figure  
 560 7b, Pearson correlation 0.18). In fact, the regression coefficients suggest that the best  
 561 way to reconstruct the strong subsurface western Pacific warming in the 1979-2020 trend

562 is via a momentum-forced response which is more in line with large-scale cooling than  
563 warming (Figure 7c). Although the understanding gained in Equation 5 works for longer-  
564 term temperature trends, it breaks down for the more recent past.

565 The disagreement between models' and observations' SST trends over this period  
566 has been the focus of many recent studies (e.g., Wills et al., 2022; Watanabe et al., 2024);  
567 our result underlines this disagreement further. We highlight two implications of this re-  
568 sult. First, while Seager et al. (2019) and Jiang et al. (2025) emphasize how differences  
569 between observations and model mean states could impact SSTs, and although GCM  
570 mean states are certainly biased, the GCMs are clearly able to recreate most of the long-  
571 term ( $> 60$  year) subsurface temperature response to historical forcing. This fact, com-  
572 bined with recent results from Dhame et al. (2025) who showed that while higher res-  
573 olution simulations reduce mean state biases they do not necessarily simulate temper-  
574 ature trends better, suggests that mean state biases are not the only cause of disagree-  
575 ment in trends over the past 40 years. This suggests that despite equatorial mean state  
576 biases our climate models are not hopelessly unfit for the task of climate change projec-  
577 tions.

578 Second, this result suggests an important role for internal variability in recent equa-  
579 torial Pacific thermocline temperature trends: we simply cannot recreate the observed  
580 pattern of subsurface temperature since the late 1970s with our linear understanding of  
581 the ocean's response to different forcings. Even making the MF coefficient negative, con-  
582 sistent with an observed strengthening Walker circulation (L'Heureux et al., 2013), is  
583 not enough to recreate the observed dipole in the equatorial thermocline. Because our  
584 patterns are quasi-steady, internal variability is an obvious culprit. Figure 7d shows how  
585 the pattern correlation between our regression-estimated reconstruction and observational  
586 trend changes as a function of start year of the trend. Trends which start before 1975  
587 are skillfully reconstructed from our linear understanding, presumably because enough  
588 cycles of internal variability have been averaged out to clarify the response. The linear  
589 reconstruction specifically fails, however, when attempting to reconstruct trends that be-  
590 gin between 1975-2000, a period which also happens to coincide with several strong El  
591 Niño events.

592 Nevertheless, we can definitively say the dynamics we have emphasized here, decadal  
593 momentum-driven thermocline tilt, subtropical cell adjustment, and equatorial stratification-

594 induced thermocline shoaling and tilt, contribute less to the 1979-2020 trend than has  
 595 been commonly hypothesized [e.g., Figure 4 schematic of Watanabe et al. (2024)]. We  
 596 hypothesize that recent internally-driven climate variability, such as ENSO or tropical  
 597 Pacific decadal variability (Capotondi et al., 2023), which is not included in our pattern  
 598 reconstructions, has critically crafted observed subsurface equatorial Pacific temperature  
 599 trends over the past 40 years. This conclusion is in line with Jiang et al. (2024a), who  
 600 emphasize the role of the Interdecadal Pacific Oscillation on SST patterns over that same  
 601 period.

### 602 4.3 Implications for the Canonical Ocean Dynamical Thermostat

603 The simplicity of this linear understanding allows us to interrogate the canonical  
 604 view of the ocean-tunnel-mediated ocean dynamical thermostat as a mechanism for un-  
 605 derstanding recent equatorial Pacific climate change. In this view, which largely rests  
 606 on a mean advective understanding of the STCs ( $\bar{v}\theta'$ ), anomalous subtropical warming  
 607 is communicated to the equatorial thermocline after some lag to erode the relative cool-  
 608 ing initially created by continued mean upwelling of unperturbed waters. As such, the  
 609 conventional view of the ocean dynamical thermostat mechanism has been limited to a  
 610 transient phenomenon. This understanding has been used to suggest that while the trop-  
 611 ical Pacific's response to climate change may start as La Niña-like, as in recent obser-  
 612 vations, it will eventually transition to El Niño-like as suggested by the vast majority  
 613 of model projections (Heede et al., 2020, 2021; Watanabe et al., 2024).

614 Our remote, buoyancy-driven response indeed shows that subtropical SST warm-  
 615 ing in the extratropics coherently warms the thermocline. While Luongo et al. (2025)  
 616 show that this pattern is best understood as having been created by wave dynamics, the  
 617 basic understanding that subtropical SSTs warm the equatorial thermocline via the STCs  
 618 holds true. In the framework of the upwelling damping effect of mean vertical advection  
 619 on equatorial SSTs ( $-\bar{w}\theta'_z \equiv -\bar{w}\frac{\theta'_s - \theta'_e}{H_e}$ : e.g., Xie et al., 2010), where the  $s$  and  $e$  sub-  
 620 scripts are respectively surface and entrainment levels and  $H_e$  is the depth of the entrain-  
 621 ment level to the surface, initially  $\theta'_e < \theta'_s$  and so mean upwelling cools, but eventually  
 622  $\theta'_e > \theta'_s$  and mean upwelling warms.

623 However, our remote and local MITgcm simulations show that this is a delicate bal-  
 624 ance: the remotely-driven thermocline warming is entirely canceled out by the locally-  
 625 driven thermocline cooling (c.f. Figures 3b, 4c, 4d). In the case of our simulations, sub-

626 tropical warming only works to erode the local cooling from thermocline shoaling and  
 627 decreased thermocline tilt such that the final, steady thermocline temperature response  
 628 is near-zero ( $\theta'_e \approx 0$ ) and there is no sign change in  $-\overline{w}\theta'_z$  with time. This implies a long-  
 629 lasting upwelling damping effect, a permanent ocean dynamical thermostat. Our model  
 630 simulations, therefore, suggest that the canonical view of the thermostat necessarily lead-  
 631 ing to a transient response (as has been used to explain recent observations) is mislead-  
 632 ing. Rather, we emphasize that the relative ratio of tropically-driven cooling to extratropically-  
 633 driven warming is critical to understand timescales associated with the buoyancy-driven  
 634 response. In our case, which in turn resembles the near-steady, centennial response to  
 635 abrupt quadrupling of CO<sub>2</sub> (Heede et al., 2021), remote warming simply cancels out lo-  
 636 cal cooling such that there is no major warming of the thermocline from SST forcing at  
 637 all (Figures 2b & 3b). If instead, however, the extratropically-driven warming was much  
 638 larger than the tropically-driven cooling we might expect a correlation between subtrop-  
 639 ical to tropical meridional SST gradients and the tropical zonal SST gradient (Burls &  
 640 Fedorov, 2014). Considered together, we instead hypothesize that the more likely driver  
 641 of transience in the surface response results from a change in the momentum-driven pat-  
 642 tern or other atmospheric pathways.

#### 643 **4.4 Symmetry of Equatorial Responses**

644 A final surprising detail of this study is the immutability of the equatorial Pacific's  
 645 subsurface temperature response regardless of forcing geography. This is best seen by  
 646 comparing the FC, BF, and MF responses to abrupt quadrupling of CO<sub>2</sub> (Figure 2) to  
 647 those same responses to NH and SH ETINMIP forcing (Figure S3). Despite the fact that  
 648 CO<sub>2</sub> forcing is primarily equatorially symmetric and ETINMIP forcing is purposefully  
 649 equatorially asymmetric, the response patterns are effectively the same (with an oppo-  
 650 site sign). From the perspective of the equatorial Pacific subsurface, it would be diffi-  
 651 cult to immediately tell the difference between greenhouse gas warming and a hypothet-  
 652 ical extratropical warming (e.g., Tseng et al., 2023). This similarity extends to the lin-  
 653 ear partitioning of the buoyancy-driven response into remote and local forcing (Figure  
 654 S4). The equatorially symmetric nature of the equatorial thermocline's response to sub-  
 655 tropical forcing (Luongo et al., 2025) creates the same remote response pattern as if both  
 656 hemispheres' subtropics were forced. Because the local response just depends on an in-  
 657 crease or decrease in surface stratification, the equatorial response to local forcing looks  
 658 effectively the same.

659 This understanding raises two interesting points. First, it highlights that hemispheric  
 660 asymmetries in meridional forcing, crucial to the zonal-mean energetic framework through  
 661 which we understand ITCZ shifts (Kang et al., 2008) and cross-equatorial ocean heat  
 662 transport (Luongo et al., 2022), do not lead to appreciably different equatorial temper-  
 663 ature responses. Despite the fact that ETINMIP forcing drives strong cross-equatorial  
 664 responses, the equatorial thermocline simply cares if the forcing causes large-scale warm-  
 665 ing or cooling. Second, the equatorial thermocline’s response to industrial aerosol forc-  
 666 ing (similar to NH ETINMIP forcing) would not lead to an independent temperature  
 667 pattern from greenhouse gas forcing. Put another way, NH aerosol forcing would sim-  
 668 ply modulate the tropical Pacific’s response to greenhouse gas forcing rather than cre-  
 669 ate a fundamentally different pattern.

## 670 5 Conclusions

671 In this study we have used a series of climate modeling simulations of varied com-  
 672 plexity to understand the equatorial thermocline response to climate change. We first  
 673 show that a multi-model mean of 11 large ensembles reasonably captures the observed  
 674 1958-2020 subsurface equatorial temperature trend, and that CESM1’s 11-50 year av-  
 675 erage response to abrupt quadrupling of CO<sub>2</sub> is an appropriate tool with which to un-  
 676 derstand the models’ response to realistic, historical forcing. We then decompose the full  
 677 equatorial thermocline response into a response due to buoyancy forcing alone and mo-  
 678 mentum forcing alone, ascribing the latter to decadal momentum dynamics. We use an  
 679 ocean-only GCM with anomalous SST forcing to further decompose that buoyancy-forced  
 680 component, and we demonstrate that the response due to extratropical SST forcing and  
 681 tropical SST forcing linearly combine to recreate the full field buoyancy-forced response.  
 682 The remote, extratropically-driven response leads to a coherent thermocline warming through  
 683 dynamic and thermodynamic pathways. The increase in near-surface stratification in the  
 684 local, tropically-driven response leads to both a shoaling thermocline and a relaxation  
 685 of thermocline tilt. Our primary finding is that a simple linear combination of these ad-  
 686 justments, i) momentum-driven, ii) remote buoyancy-driven, and iii) local buoyancy-driven,  
 687 skillfully explains both the long-term 1958-2020 modeled and observed responses. We  
 688 can attribute certain features of the pattern to certain dynamics: we agree with Vecchi  
 689 and Soden (2007) and Jiang et al. (2025)’s suggestion that the thermocline cooling re-  
 690 sponse to global warming results from momentum-driven dynamics. However, this dy-

691 namical understanding does not explain more recent trends (e.g., the 1979-2020 response),  
692 suggesting that this period was strongly affected by internal variability.

693 Our results emphasize that the subsurface equatorial Pacific temperature response  
694 to climate change is a highly linear system. This linearity is powerful. It allows us to test  
695 long-held theoretical understandings, such as how subtropical warming will affect the tran-  
696 sient adjustment of the tropical thermocline or that changes in zonal wind stress are nec-  
697 essary for a thermocline tilt. While this study does not answer what has caused recent  
698 subsurface mismatches between models and observations or whether models are miss-  
699 ing a hypothetical forcing that might explain that mismatch, we demonstrate that model  
700 mean states are not so irreparably biased that we cannot learn from them. Instead, these  
701 models clarify the specific patterns created by commonly referenced ocean dynamic ad-  
702 justments. In a practical sense, we also outline a clear model hierarchy, fully-coupled,  
703 mechanically-decoupled, ocean-only, and reduced gravity, which could be potentially lever-  
704 aged to comprehend other coupled climate responses.

## 705 **6 Open Research**

706 The climate model output and python RG model used in this study will be made  
707 freely available upon study publication by the corresponding author.

## 708 **Acknowledgments**

709 MTL was supported by the Cooperative Institute for Climate, Ocean, & Ecosystem Stud-  
710 ies (CICOES) under NOAA Cooperative Agreement XX, Contribution No. XX. IE was  
711 supported by National Science Foundation (NSF) award OCE-2048590. KCA was sup-  
712 ported by NSF award AGS-2203543 and a Calvin Professorship in Oceanography. We  
713 thank UCAR and NSF for providing an exploratory allocation of core hours on the Cheyenne  
714 and Derecho supercomputers. We sincerely thank Feng Jiang for providing the ensem-  
715 ble mean model data used in Figure 1b & d, and without implying endorsement, we thank  
716 Natalie Burls for helpful discussion.

## 717 **References**

- 718 Baldwin, J. W., Atwood, A. R., Vecchi, G. A., & Battisti, D. S. (2021). Outsize  
719 Influence of Central American Orography on Global Climate. *AGU Advances*,  
720 *2*(2), e2020AV000343.  
721 Bjerknes, J. (1969). Atmospheric Teleconnections from the Equatorial Pacific.

- 722            *Monthly weather review*, *97*(3), 163–172.
- 723    Burls, N., & Fedorov, A.    (2014).    What Controls the Mean East–West Sea Surface  
724            Temperature Gradient in the Equatorial Pacific: The Role of Cloud Albedo.  
725            *Journal of Climate*, *27*(7), 2757–2778.
- 726    Capotondi, A., McGregor, S., McPhaden, M. J., Cravatte, S., Holbrook, N. J.,  
727            Imada, Y., . . . others (2023). Mechanisms of Tropical Pacific Decadal Variabil-  
728            ity. *Nature Reviews Earth & Environment*, *4*(11), 754–769.
- 729    Carton, J. A., & Giese, B. S.    (2008).    A Reanalysis of Ocean Climate Using Sim-  
730            ple Ocean Data Assimilation (SODA). *Monthly weather review*, *136*(8), 2999–  
731            3017.
- 732    Clement, A. C., Seager, R., Cane, M. A., & Zebiak, S. E. (1996). An Ocean Dynam-  
733            ical Thermostat. *Journal of Climate*, *9*(9), 2190–2196.
- 734    Coats, S., & Karnauskas, K.    (2017).    Are Simulated and Observed Twentieth Cen-  
735            tury Tropical Pacific Sea Surface Temperature Trends Significant Relative to  
736            Internal Variability? *Geophysical Research Letters*, *44*(19), 9928–9937.
- 737    Dhame, S., Olonscheck, D., & Rugenstein, M.    (2025).    Higher-Resolution Climate  
738            Models Do Not Consistently Reproduce the Observed Tropical Pacific Warm-  
739            ing Pattern. *Journal of Climate*, *38*(13), 3131–3149.
- 740    DiNezio, P. N., Clement, A. C., Vecchi, G. A., Soden, B. J., Kirtman, B. P., & Lee,  
741            S.-K.    (2009).    Climate Response of the Equatorial Pacific to Global Warming.  
742            *Journal of Climate*, *22*(18), 4873–4892.
- 743    Dong, Y., Armour, K. C., Battisti, D. S., & Blanchard-Wrigglesworth, E.    (2022).  
744            Two-way Teleconnections between the Southern Ocean and the Tropical Pa-  
745            cific via a Dynamic Feedback. *Journal of Climate*, *35*(19), 6267–6282.
- 746    Forget, G., Campin, J.-M., Heimbach, P., Hill, C., Ponte, R., & Wunsch, C.    (2015).  
747            ECCO Version 4: An Integrated Framework for Non-Linear Inverse Modeling  
748            and Global Ocean State Estimation. *Geoscientific Model Development*, *8*(10),  
749            3071–3104.
- 750    Good, S. A., Martin, M. J., & Rayner, N. A.    (2013).    EN4: Quality Controlled  
751            Ocean Temperature and Salinity Profiles and Monthly Objective Analyses with  
752            Uncertainty Estimates. *Journal of Geophysical Research: Oceans*, *118*(12),  
753            6704–6716.
- Heede, U. K., & Fedorov, A. V.            (2021).            Eastern Equatorial Pa-

- cific Warming Delayed by Aerosols and Thermostat Response to  
 CO<sub>2</sub> Increase. *Nature Climate Change*, *11*(8), 696 – –703.
- 754 Heede, U. K., & Fedorov, A. V. (2023). Colder Eastern Equatorial Pacific and  
 755 Stronger Walker Circulation in the Early 21st Century: Separating the Forced  
 756 Response to Global Warming from Natural Variability. *Geophysical Research*  
 757 *Letters*, *50*(3), e2022GL101020.
- 758 Heede, U. K., Fedorov, A. V., & Burls, N. J. (2020). Time Scales and Mechanisms  
 759 for the Tropical Pacific Response to Global Warming: A Tug of War between  
 760 the Ocean Thermostat and Weaker Walker. *Journal of Climate*, *33*(14), 6101–  
 761 6118.
- 762 Heede, U. K., Fedorov, A. V., & Burls, N. J. (2021). A Stronger versus Weaker  
 763 Walker: Understanding Model Differences in Fast and Slow Tropical Pacific  
 764 Responses to Global Warming. *Climate Dynamics*, *57*(9), 2505–2522.
- 765 Horel, J. D., & Wallace, J. M. (1981). Planetary-scale Atmospheric Phenomena As-  
 766 sociated with the Southern Oscillation. *Monthly Weather Review*, *109*(4), 813–  
 767 829.
- 768 Hurrell, J. W., Holland, M. M., Gent, P. R., Ghan, S., Kay, J. E., Kushner, P. J.,  
 769 ... others (2013). The Community Earth System Model: A Framework for  
 770 Collaborative Research. *Bulletin of the American Meteorological Society*,  
 771 *94*(9), 1339–1360.
- 772 Hwang, Y.-T., Xie, S.-P., Chen, P.-J., Tseng, H.-Y., & Deser, C. (2024). Contri-  
 773 bution of Anthropogenic Aerosols to Persistent La Niña-like Conditions in the  
 774 Early 21st Century. *Proceedings of the National Academy of Sciences*, *121*(5),  
 775 e2315124121.
- 776 Ishii, M., & Kimoto, M. (2009). Reevaluation of Historical Ocean Heat Content  
 777 Variations with Time-Varying XBT and MBT Depth Bias Corrections. *Journal*  
 778 *of Oceanography*, *65*(3), 287–299.
- 779 Jiang, F., Seager, R., & Cane, M. A. (2024a). A Climate Change Signal in the Trop-  
 780 ical Pacific Emerges from Decadal Variability. *Nature Communications*, *15*(1),  
 781 8291.
- 782 Jiang, F., Seager, R., & Cane, M. A. (2024b). Historical Subsurface Cooling in the  
 783 Tropical Pacific and its Dynamics. *Journal of Climate*, *37*(22), 5925–5938.
- 784 Jiang, F., Seager, R., Cane, M. A., Karamperidou, C., & Brizuela, N. G. (2025).

- 785           Subsurface Cooling and Sea Surface Temperature Pattern Formation over  
786           the Equatorial Pacific.       *Journal of Geophysical Research: Oceans*, 130(4),  
787           e2024JC022222.
- 788    Ju, W.-S., Zhang, Y., & Du, Y. (2022). Subsurface Cooling in the Tropical Pacific  
789           under a Warming Climate.   *Journal of Geophysical Research: Oceans*, 127(5),  
790           e2021JC018225.
- 791    Kang, S. M., Hawcroft, M., Xiang, B., Hwang, Y.-T., Cazes, G., Codron, F., ...  
792           others (2019). Extratropical–Tropical Interaction Model Intercomparison  
793           Project (ETIN-MIP): Protocol and Initial Results.   *Bulletin of the American*  
794           *Meteorological Society*, 100(12), 2589–2606.
- 795    Kang, S. M., Held, I. M., Frierson, D. M., & Zhao, M. (2008). The Response of the  
796           ITCZ to Extratropical Thermal Forcing: Idealized Slab-Ocean Experiments  
797           with a GCM. *Journal of Climate*, 21(14), 3521–3532.
- 798    Kang, S. M., Shin, Y., Kim, H., Xie, S.-P., & Hu, S. (2023). Disentangling the  
799           Mechanisms of Equatorial Pacific Climate Change.   *Science Advances*, 9(19),  
800           eadf5059.
- 801    Karnauskas, K. B., Seager, R., Kaplan, A., Kushnir, Y., & Cane, M. A. (2009).  
802           Observed Strengthening of the Zonal Sea Surface Temperature Gradient across  
803           the Equatorial Pacific Ocean. *Journal of Climate*, 22(16), 4316–4321.
- 804    Knutson, T. R., & Manabe, S. (1995). Time-mean Response  
805           over the Tropical Pacific to Increased CO<sub>2</sub> in a Coupled Ocean –  
806           Atmosphere Model. *Journal of Climate*, 8(9), 2181 – 2199.
- 807    Kosaka, Y., & Xie, S.-P. (2016). The Tropical Pacific as a Key Pacemaker of the  
808           Variable Rates of Global Warming. *Nature Geoscience*, 9(9), 669–673.
- 809    Laepple, T., & Huybers, P. (2014). Ocean Surface Temperature Variability: Large  
810           Model-Data Differences at Decadal and Longer Periods. *Proceedings of the Na-*  
811           *tional Academy of Sciences*, 111(47), 16682–16687.
- 812    Liu, Z. (1994). A Simple Model of the Mass Exchange between the Subtropical and  
813           Tropical Ocean. *Journal of Physical Oceanography*, 24(6), 1153–1165.
- 814    Luo, Y., Liu, F., & Lu, J. (2018). Response of the Equatorial Pacific Thermocline to  
815           Climate Warming. *Ocean Dynamics*, 68(11), 1419–1429.
- 816    Luo, Y., Lu, J., Liu, F., & Garuba, O. (2017). The Role of Ocean Dynamical Ther-  
817           mostat in Delaying the El Niño-like Response over the Equatorial Pacific to

- 815 Climate Warming. *Journal of Climate*, *30*(8), 2811–2827.
- 816 Luo, Y., Rothstein, L. M., & Zhang, R.-H. (2009). Response of Pacific Subtropical-  
817 Tropical Thermocline Water Pathways and Transports to Global Warming.  
818 *Geophysical Research Letters*, *36*(4).
- 819 Luongo, M. T., Brizuela, N. G., Eisenman, I., & Xie, S.-P. (2024). Retaining  
820 Short-term Variability Reduces Mean State Biases in Wind Stress Overrid-  
821 ing Simulations. *Journal of Advances in Modeling Earth Systems*, *16*(2),  
822 e2023MS003665.
- 823 Luongo, M. T., Xie, S.-P., & Eisenman, I. (2022). Buoyancy forcing dominates  
824 the cross-equatorial ocean heat transport response to Northern Hemisphere  
825 extratropical cooling. *Journal of Climate*, *35*(20), 6671–6690.
- 826 Luongo, M. T., Xie, S.-P., Eisenman, I., Hwang, Y.-T., & Tseng, H.-Y. (2023). A  
827 Pathway for Northern Hemisphere Extratropical Cooling to Elicit a Tropical  
828 Response. *Geophysical Research Letters*, *50*(2), e2022GL100719.
- 829 Luongo, M. T., Xie, S.-P., Eisenman, I., Sun, S., & Peng, Q. (2025). How the Sub-  
830 surface Tropical Pacific Responds to Subtropical Surface Cooling: Implications  
831 for Cross-Equatorial Transport. *Journal of Climate*.
- 832 L’Heureux, M. L., Lee, S., & Lyon, B. (2013). Recent Multidecadal Strengthening  
833 of the Walker Circulation across the Tropical Pacific. *Nature Climate Change*,  
834 *3*(6), 571–576.
- 835 Mantua, N. J., Hare, S. R., Zhang, Y., Wallace, J. M., & Francis, R. C. (1997). A  
836 Pacific Interdecadal Climate Oscillation with Impacts on Salmon Production.  
837 *Bulletin of the American Meteorological Society*, *78*(6), 1069–1080.
- 838 McCreary Jr, J. P., & Lu, P. (1994). Interaction between the Subtropical and Equa-  
839 torial Ocean Circulations: The Subtropical Cell. *Journal of Physical Oceanog-  
840 raphy*, *24*(2), 466–497.
- 841 McGregor, S., Stuecker, M. F., Kajtar, J. B., England, M. H., & Collins, M. (2018).  
842 Model Tropical Atlantic Biases Underpin Diminished Pacific Decadal Variabil-  
843 ity. *Nature Climate Change*, *8*(6), 493–498.
- 844 Merlis, T. M., & Schneider, T. (2011). Changes in Zonal Surface Temperature Gra-  
845 dients and Walker Circulations in a Wide Range of Climates. *Journal of cli-  
846 mate*, *24*(17), 4757–4768.
- 847 Olonscheck, D., Rugenstein, M., & Marotzke, J. (2020). Broad Consistency be-

- 848           tween Observed and Simulated Trends in Sea Surface Temperature Patterns.  
849           *Geophysical Research Letters*, 47(10), e2019GL086773.
- 850 Peng, Q., Xie, S.-P., Wang, D., Huang, R. X., Chen, G., Shu, Y., ... Liu, W. (2022).  
851           Surface Warming-Induced Global Acceleration of Upper Ocean Currents. *Sci-*  
852           *ence Advances*, 8(16), eabj8394.
- 853 Philander, S. G. H. (1983). El Niño Southern Oscillation Phenomena. *Nature*,  
854           302(5906), 295–301.
- 855 Seager, R., Cane, M., Henderson, N., Lee, D.-E., Abernathey, R., & Zhang, H.  
856           (2019). Strengthening Tropical Pacific Zonal Sea Surface Temperature Gradi-  
857           ent Consistent with Rising Greenhouse Gases. *Nature Climate Change*, 9(7),  
858           517–522.
- 859 Seager, R., Henderson, N., & Cane, M. (2022). Persistent Discrepancies between Ob-  
860           served and Modeled Trends in the Tropical Pacific Ocean. *Journal of Climate*,  
861           35(14), 4571–4584.
- 862 Seager, R., & Murtugudde, R. (1997). Ocean Dynamics, Thermocline Adjustment,  
863           and Regulation of Tropical SST. *Journal of climate*, 10(3), 521–534.
- 864 Solomon, A., & Newman, M. (2012). Reconciling Disparate Twentieth-century Indo-  
865           Pacific Ocean Temperature Trends in the Instrumental Record. *Nature Climate*  
866           *Change*, 2(9), 691–699.
- 867 Sun, S., & Thompson, A. F. (2020). Centennial Changes in the Indonesian Through-  
868           flow Connected to the Atlantic Meridional Overturning Circulation: The  
869           Ocean’s Transient Conveyor Belt. *Geophysical Research Letters*, 47(21),  
870           e2020GL090615.
- 871 Taylor, B. A., Shi, J.-R., Xie, S.-P., Talley, L. D., Luongo, M. T., & Peng, Q. (2025).  
872           Warming Band in Southern Ocean’s Indian Sector: The Role of Remote At-  
873           lantic Buoyancy Forcing via Poleward-Shifting Circulation Response. *Journal*  
874           *of Climate*, 38(14), 3219–3238.
- 875 Tseng, H.-Y., Hwang, Y.-T., Xie, S.-P., Tseng, Y.-H., Kang, S. M., Luongo, M. T.,  
876           & Eisenman, I. (2023). Fast and Slow Responses of the Tropical Pacific to  
877           Radiative Forcing in Northern High Latitudes. *Journal of Climate*, 36(16),  
878           5337–5349.
- 879 Tuchen, F. P., Perez, R. C., Foltz, G. R., McPhaden, M. J., & Lumpkin, R. (2024).  
880           Strengthening of the Equatorial Pacific Upper-Ocean Circulation over the

- 881 Past Three Decades. *Journal of Geophysical Research: Oceans*, 129(11),  
882 e2024JC021343.
- 883 Vecchi, G. A., & Soden, B. J. (2007). Global Warming and the Weakening of the  
884 Tropical Circulation. *Journal of Climate*, 20(17), 4316–4340.
- 885 Watanabe, M., Dufresne, J.-L., Kosaka, Y., Mauritsen, T., & Tatebe, H. (2021). En-  
886 hanced Warming Constrained by Past Trends in Equatorial Pacific Sea Surface  
887 Temperature Gradient. *Nature Climate Change*, 11(1), 33–37.
- 888 Watanabe, M., Kang, S. M., Collins, M., Hwang, Y.-T., McGregor, S., & Stuecker,  
889 M. F. (2024). Possible Shift in Controls of the Tropical Pacific Surface Warm-  
890 ing Pattern. *Nature*, 630(8016), 315–324.
- 891 Wills, R. C., Dong, Y., Proistosescu, C., Armour, K. C., & Battisti, D. S. (2022).  
892 Systematic Climate Model Biases in the Large-scale Patterns of Recent Sea-  
893 surface Temperature and Sea-level Pressure Change. *Geophysical Research*  
894 *Letters*, 49(17), e2022GL100011.
- 895 Wyrski, K. (1975). El Niño—The Dynamic Response of the Equatorial Pacific  
896 Ocean to Atmospheric Forcing. *Journal of Physical Oceanography*, 5(4), 572–  
897 584.
- 898 Xie, S.-P., Deser, C., Vecchi, G. A., Ma, J., Teng, H., & Wittenberg, A. T. (2010).  
899 Global Warming Pattern Formation: Sea Surface Temperature and Rainfall.  
900 *Journal of Climate*, 23(4), 966–986.
- 901 Yang, H., Wang, F., & Sun, A. (2009). Understanding the ocean temperature change  
902 in global warming: the tropical Pacific. *Tellus A: Dynamic Meteorology and*  
903 *Oceanography*, 61(3), 371–380.
- 904 Zuo, H., Balmaseda, M. A., Tietsche, S., Mogensen, K., & Mayer, M. (2019). The  
905 ECMWF Operational Ensemble Reanalysis–Analysis System for Ocean and  
906 Sea Ice: A Description of the System and Assessment. *Ocean science*, 15(3),  
907 779–808.

# Supporting Information for “Explaining the Equatorial Pacific Thermocline Response to Climate Change with a Model Hierarchy”

Matthew T. Luongo<sup>1,2</sup>, Shang-Ping Xie<sup>3</sup>, Ian Eisenman<sup>3</sup>, Shantong Sun<sup>4</sup>, &

Kyle C. Armour<sup>2,5</sup>

<sup>1</sup>Cooperative Institute for Climate, Ocean, & Ecosystem Studies, University of Washington, Seattle, WA

<sup>2</sup>School of Oceanography, University of Washington, Seattle, WA

<sup>3</sup>Scripps Institution of Oceanography, UC San Diego, La Jolla, CA

<sup>4</sup>Laoshan Laboratory, Qingdao, China

<sup>5</sup>Department of Atmospheric & Climate Science, University of Washington, Seattle, WA

**Contents of this file** Table S1 and Figures S1-S4

## References

- Carton, J. A., & Giese, B. S. (2008). A Reanalysis of Ocean Climate Using Simple Ocean Data Assimilation (SODA). *Monthly weather review*, *136*(8), 2999–3017.
- Good, S. A., Martin, M. J., & Rayner, N. A. (2013). EN4: Quality Controlled Ocean Temperature and Salinity Profiles and Monthly Objective Analyses with Uncertainty Estimates. *Journal of Geophysical Research: Oceans*, *118*(12), 6704–6716.
- Ishii, M., & Kimoto, M. (2009). Reevaluation of Historical Ocean Heat Content Variations with Time-Varying XBT and MBT Depth Bias Corrections. *Journal of Oceanography*, *65*(3), 287–299.

- Jiang, F., Seager, R., Cane, M. A., Karamperidou, C., & Brizuela, N. G. (2025). Subsurface Cooling and Sea Surface Temperature Pattern Formation over the Equatorial Pacific. *Journal of Geophysical Research: Oceans*, *130*(4), e2024JC022222.
- Kang, S. M., Hawcroft, M., Xiang, B., Hwang, Y.-T., Cazes, G., Codron, F., . . . others (2019). Extratropical–Tropical Interaction Model Intercomparison Project (ETIN-MIP): Protocol and Initial Results. *Bulletin of the American Meteorological Society*, *100*(12), 2589–2606.
- Zuo, H., Balmaseda, M. A., Tietsche, S., Mogensen, K., & Mayer, M. (2019). The ECMWF Operational Ensemble Reanalysis–Analysis System for Ocean and Sea Ice: A Description of the System and Assessment. *Ocean science*, *15*(3), 779–808.

Fully-coupled Simulations			
Simulation Name	CO <sub>2</sub> Forcing	Wind Stress	ETINMIP Forcing
ETINMIPNH	280ppm	Freely evolving	45°N–65°N
ETINMIPSH	280ppm	Freely evolving	45°S–65°S
Mechanically-decoupled Simulations			
Simulation Name	CO <sub>2</sub> Forcing	Wind Stress	ETINMIP Forcing
Tau1SNH	280ppm	Ctrl	45°N–65°N
TauNHS1	280ppm	ETINMIPNH	n/a
Tau1SSH	280ppm	Ctrl	45°S–65°S
TauSHS1	280ppm	ETINMIPSH	n/a
Ocean-only Simulations			
Simulation Name	SST Forcing Perturbation	SST Forcing Bounds	
ETINMIPNH_BFsst	Tau1SNH-Tau1CO <sub>2</sub> x1	90°S-90°N	
ETINMIPNH_BFsstET	Tau1SNH-Tau1CO <sub>2</sub> x1	90°S-6°S, 6°N-90°N	
ETINMIPNH_BFsstEQ	Tau1SNH-Tau1CO <sub>2</sub> x1	10°S-10°N	
ETINMIPSH_BFsst	Tau1SSH-Tau1CO <sub>2</sub> x1	90°S-90°N	
ETINMIPSH_BFsstET	Tau1SSH-Tau1CO <sub>2</sub> x1	90°S-6°S, 6°N-90°N	
ETINMIPSH_BFsstEQ	Tau1SSH-Tau1CO <sub>2</sub> x1	10°S-10°N	

**Table S1.** Details of fully coupled, mechanically-decoupled, and ocean-only simulations using top-of-atmosphere hemispherically asymmetric extratropical forcing from the Extratropical-Tropical Interaction Model Intercomparison Project (ETINMIP: Kang et al., 2019). The Ctrl and Tau1CO<sub>2</sub>x1 simulations are described in Table 1 of the main text.

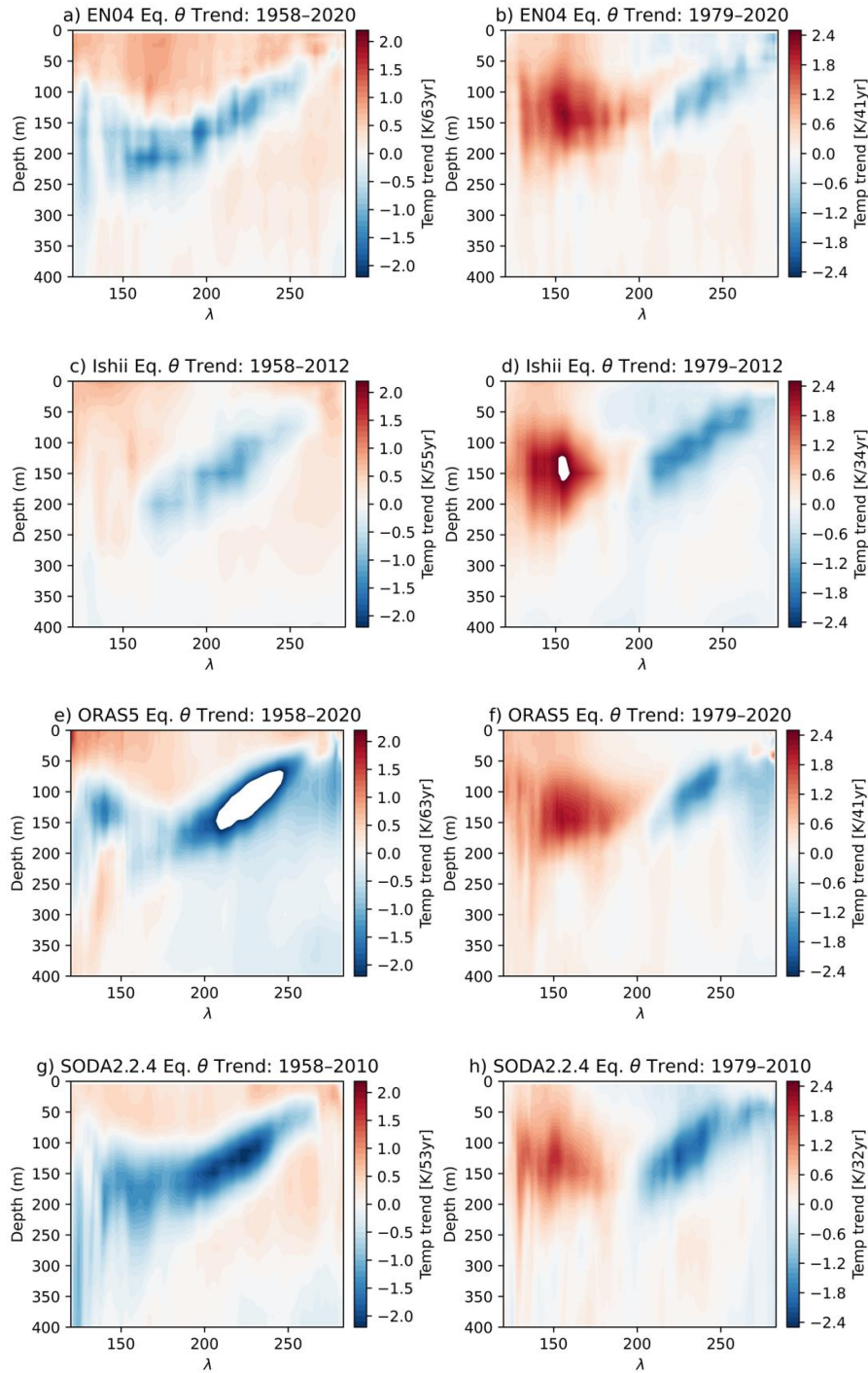


**Figure S1.** Equatorial subsurface temperature ( $\theta$ ) trend for EN04 observational product (top row, Good et al., 2013), Ishii observational product (second row, Ishii & Kimoto, 2009), ORAS5 ocean reanalysis (third row, Zuo et al., 2019), and SODA2.2.4 ocean reanalysis (fourth row, Carton & Giese, 2008) While time periods depend on specific data source, longer-term trends are in the left column and shorter-term trends in the right column.

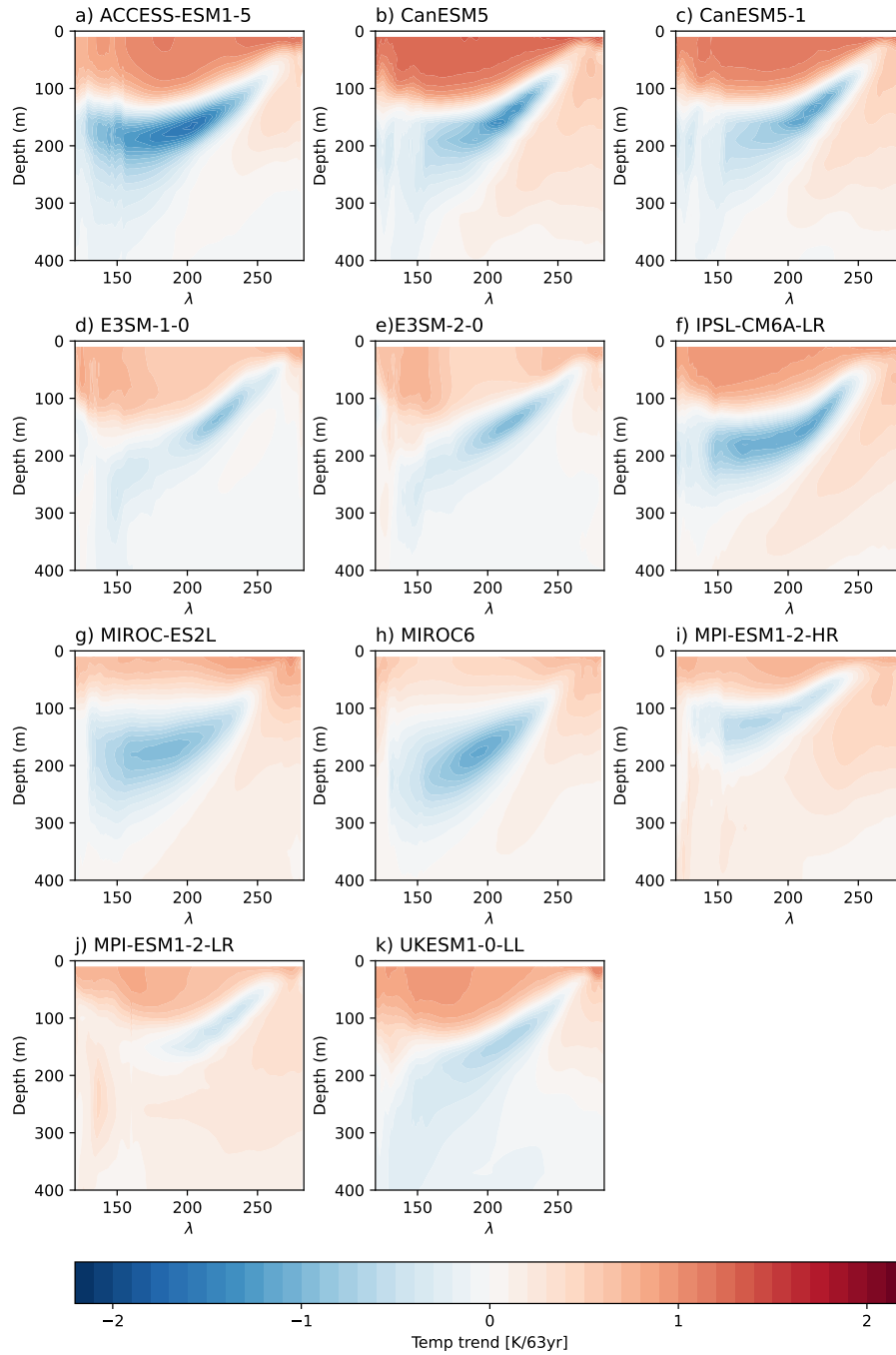


**Figure S2.** Ensemble mean 1958-2020 equatorial subsurface temperature ( $\theta$ ) trend for a) ACCESS-ESM1-5, b) CanESM5, c) CanESM5-1, d) E3SM-1-0, e) E3SM-2-0, f) IPSL-CM6A-LR, g) MIROC-ES2L, h) MIROC6, i) MPI-ESM1-2-HR, j) MPI-ESM1-2-LR, and k) UKESM1-0-LL large ensembles as selected by Jiang et al. (2025). Ensembles are forced by historical forcing from 1958-2014 and from 2015-2020 by the Shared Socioeconomic Pathway 3-7.5 scenario.

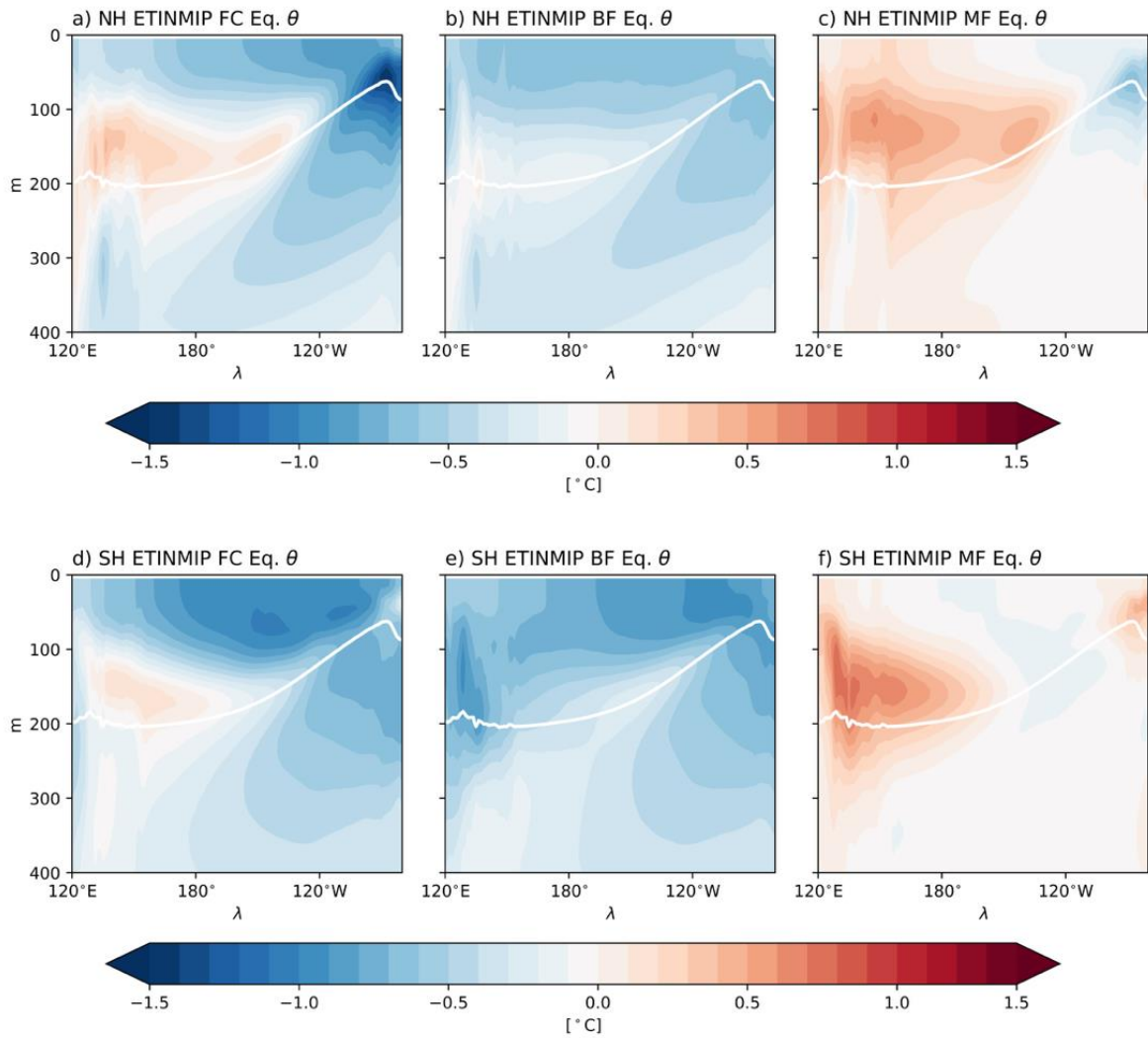


**Figure S3.** a) CESM1 fully-coupled (FC = ETINMIPNH-Ctrl) equatorial temperature ( $\theta$ ) response to Northern Hemisphere (NH) ETINMIP forcing. b) CESM1 buoyancy-forced (BF = Tau1SNH-Tau1CO<sub>2</sub>x1) equatorial  $\theta$  response to NH ETINMIP forcing. c) CESM1 momentum-forced (MF = TauNHS1-Tau1CO<sub>2</sub>x1) equatorial  $\theta$  response to NH ETINMIP forcing. d) CESM1 FC (ETINMIPSH-Ctrl) equatorial  $\theta$  response to Southern Hemisphere (SH) ETINMIP forcing. e) CESM1 BF (Tau1SSH-Tau1CO<sub>2</sub>x1) equatorial  $\theta$  response to SH ETINMIP forcing. f) CESM1 MF (TauSHS1-Tau1CO<sub>2</sub>x1) equatorial  $\theta$  response to SH ETINMIP forcing. All panels are meridionally averaged from 5°S-5°N, temporally averaged from years 11-50, and they show the 16°C isotherm from the Ctrl simulation as a white contour to approximate the thermocline.

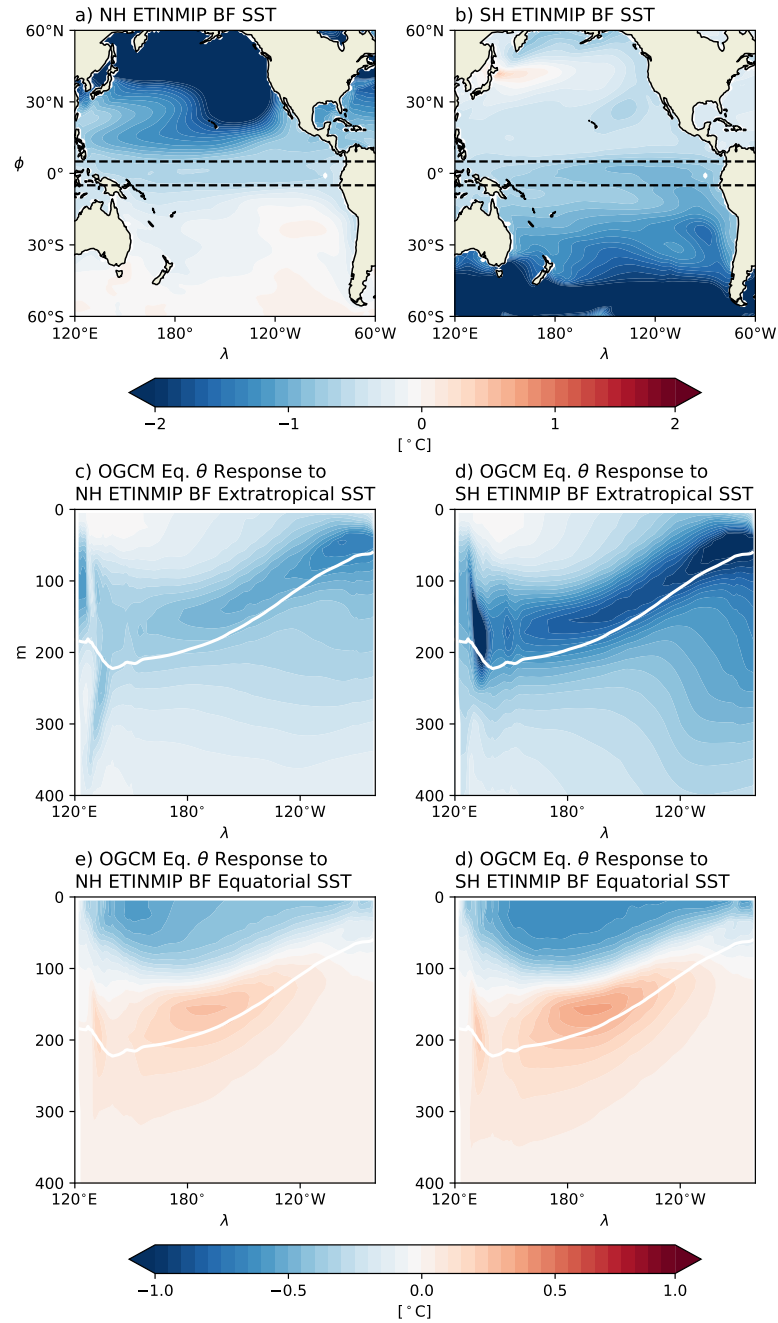


**Figure S4.** a) NH ETINMIP BF SST pattern from CESM1. b) SH ETINMIP BF SST pattern from CESM1. c) Equatorial  $\theta$  response to remote NH ETINMIP BF SST forcing. d) Equatorial  $\theta$  response to remote SH ETINMIP BF SST forcing. e) Equatorial  $\theta$  response to local NH ETINMIP BF SST forcing. d) Equatorial  $\theta$  response to local SH ETINMIP BF SST forcing. Dashed black lines in the top row correspond to the bounds that we separate the local and remote responses by.